Distinct checkpoint and homolog biorientation pathways regulate meiosis I in *Drosophila* oocytes

Joanatta G. Shapiro, Neha Changela, Janet K. Jang, Jay N. Joshi, and Kim S. McKim

Waksman Institute and Department of Genetics, Rutgers, the State University of New Jersey, Piscataway, New Jersey, United States of America.

Condensed title: Checkpoint and biorientation pathways in oocytes

Correspondence: Kim S. McKim (mckim@waksman.rutgers.edu)

Corresponding author: Kim S. McKim
190 Frelinghuysen Road,
Piscataway, NJ-08854
848-445-1164
mckim@waksman.rutgers.edu

Abstract

Mitosis and meiosis have two mechanisms for regulating the accuracy of chromosome segregation: error correction and the spindle assembly checkpoint (SAC). We have investigated the function of several checkpoint proteins in meiosis I of *Drosophila* oocytes. Evidence of a SAC response by several of these proteins is found upon depolymerization of microtubules by colchicine. However, unattached kinetochores or errors in biorientation of homologous chromosomes does not induce a SAC response. Furthermore, the metaphase I arrest does not depend on SAC genes, suggesting the APC is inhibited even if the SAC is silenced. Two SAC proteins, ROD of the ROD-ZW10-Zwilch (RZZ) complex and MPS1, are also required for the biorientation of homologous chromosomes during meiosis I, suggesting an error correction function. Both proteins aid in preventing or correcting erroneous attachments and depend on SPC105R for localization to the kinetochore. We have defined a region of SPC105R, amino acids 123-473, that is required for ROD localization and biorientation of homologous chromosomes at meiosis I. Surprisingly, ROD removal, or “streaming”, is independent of the dynein adaptor Spindly and is not linked to the stabilization of end-on attachments. Instead, meiotic RZZ streaming appears to depend on cell cycle stage and may be regulated independently of kinetochore attachment or biorientation status. We also show that dynein adaptor Spindly is also required for biorientation at meiosis I, and surprisingly, the direction of RZZ streaming.

Author Summary

The Spindle Assembly Checkpoint (SAC) is known to delay cell cycle progression until chromosomes are properly attached to microtubules. Meiotic cells often have modified cell cycle phases, and natural arrest points such as metaphase I in *Drosophila*. We show that in *Drosophila* oocytes, the SAC is sensitive to loss of microtubules, but not sensitive to a variety of kinetochore attachment errors. Thus, the function of the SAC appears to be limited to monitoring oocyte spindle assembly, and not required for accurate chromosome segregation. However, two of the SAC genes, *rod* and *Mps1*, are required for the biorientation of homologous chromosomes during meiosis I, suggesting an error correction function. Rod is part of the RZZ complex and is notable for its property of streaming off the kinetochores. However, our results show that streaming off the kinetochore may not contribute to RZZ regulation of microtubule attachments, and only be associated with SAC function. Instead, the establishment of stable end-on attachments may occur while RZZ is still present at kinetochore. We suggest that RZZ interacts with multiple motors to promote bidirectional movement of kinetochores along microtubules, which allows chromosomes to find and attach to the correct pole.

60 # Introduction

61 Errors during meiotic chromosome segregation can result in inviable gametes
62 leading to spontaneous abortions and infertility, or viable offspring with chromosomal
63 abnormalities. Several mechanisms exist in dividing cells to prevent aneuploidy
64 resulting from improper kinetochore-microtubule (KT-MT) attachments. The spindle
65 assembly checkpoint (SAC) delays anaphase onset until attachments form between
66 kinetochores and microtubules [1, 2]. Unattached kinetochores generate a signal
67 involving SAC proteins such as MAD1, MAD2, BUB1, and BUB3 that have a global
68 effect on all chromosomes and cell cycle progression. In contrast, error correction (EC)
69 is specific to individual kinetochores whereupon interactions between microtubules and
70 properly bi-oriented kinetochores are stabilized while those with improperly oriented
71 kinetochores are weakened [3]. Multiple models have been proposed to explain how
72 improperly oriented kinetochores are identified, involving both tension-dependent and -
73 independent mechanisms, and how they are corrected, including phosphorylation of
74 kinetochore proteins to destabilize attachments [4, 5].

75 Error rates are higher in human oocytes than in spermatocytes, which has been
76 attributed to several causes [6-8]. One hypothesis is that the SAC is weak or inefficient
77 [7, 9-11]. Indeed, Xenopus oocytes may not have a functional SAC [12, 13]. The
78 observation that mammalian oocytes progress through anaphase with segregation
79 errors may be a result of a weak checkpoint [14, 15]. The reason for a weak SAC in
80 oocytes is not known, although possible contributing factors include the large size of
81 oocytes or the lack of centrosomes [9, 16-19]. The SAC may also have other functions

82 in oocytes, such as regulating the development of the oocytes and the timing of meiotic
83 progression [10].[1, 2].
84 *Drosophila* oocytes are an excellent model for studying meiosis in females, but
85 the SAC has not been examined. *Drosophila* oocytes have kinetochores that include the
86 KMN complex (KNL1-MIS12-NDC80) [20]. Biorientation of homologous chromosomes
87 involves types of kinetochore-microtubule attachments, lateral attachments that depend
88 on KNL1/SPC105R and end-on attachments that depend on NDC80 [21, 22]. To
89 understand the contributions of SAC and EC to biorientation in *Drosophila* oocytes, we
90 characterized the SAC response during the first meiotic division, investigated how the
91 SAC proteins are recruited to the kinetochores, and tested several SAC proteins for
92 functions in meiotic EC. Our data suggest that the SAC is not sensitive to kinetochore
93 attachment status and might be silenced prior to the metaphase I arrest. Furthermore,
94 among seven SAC proteins, only two, ROD of the ROD-ZW10-Zwilch (RZZ) complex
95 and MPS1, are required for biorientation of meiotic homologous chromosomes at
96 metaphase I.
97 We examined the role of RZZ in *Drosophila* oocytes because it has not been
98 studied before in meiosis. Previous studies in *C. elegans* embryos and *Drosophila*
99 neuroblasts suggest that RZZ prevents errors by inhibiting premature stabilization of
100 interactions between the ends of microtubules and NDC80 [23, 24]. RZZ also has the
101 property of streaming off the kinetochore, which could alleviate the inhibition of end-on
102 attachments [24-26]. We have shown that the RZZ complex is required for accurate
103 homolog biorientation in meiosis I, which could indicate a role for the RZZ complex in
104 delaying the formation of end-on attachments. We also show that Spindly, a dynein

105 adaptor for RZZ, is also required for homolog biorientation in meiosis I. However, RZZ
106 streaming in oocytes is not required for, nor does it depend on, the formation of end-on
107 attachments. We propose that RZZ streams in response to the silencing of the SAC
108 prior to the metaphase I arrest. Biorientation, however, depends on an interaction
109 between RZZ, Spindly, and possibly other motor activities, that regulate chromosome
110 movement and attachment status.
111

112 # Results

113 ### *Analysis of the SAC protein localization in oocytes*

114 The localization of SAC proteins was examined in *Drosophila* oocytes. Mature
115 *Drosophila* oocytes, known as stage 14, arrest at metaphase I with the chromosomes
116 clustered together in a single mass, or karyosome, and the centromeres of homologous
117 chromosomes oriented towards opposite poles. Several SAC proteins were detected at
118 kinetochores in stage 14 oocytes, including BUBR1, BUB3, MPS1 and ROD (Figure
119 1A). In addition to its kinetochore localization, ROD localized to the spindle region
120 between the pole and the centromeres (Figure 1). This redistribution of ROD from the
121 kinetochores to the spindle is termed “streaming” and has been previously observed in
122 mitotic cells [25, 27, 28]. Another RZZ subunit, ZW10 tagged with HA, overlapped with
123 ROD^{GFP} staining, validating that ROD^{GFP} provides an accurate representation of the
124 RZZ complex’s localization (Figure S 1A).

125 In contrast to the above proteins, we did not detect MAD1 in stage 14 oocytes
126 (Figure 1A). Therefore, we attempted to increase SAC signaling by incubating stage 14
127 oocytes in colchicine for 60 minutes to remove nearly all microtubules. Following this
128 treatment, robust kinetochore localization of MAD1 was observed in all oocytes (Figure
129 1B). Because colchicine induced a change in MAD1 localization, we tested if the
130 localization of other checkpoint protein was increased by loss of microtubules. BUBR1
131 and MPS1 intensity increased in colchicine, suggesting their levels are sensitive to the
132 SAC (Figure 1C). We did not, however, observe a SAC response with BUB3
133 localization.

134 A more dramatic response was observed with ROD. In colchicine-treated
135 oocytes, ROD expanded around the kinetochores (Figure 1B). In some cases, ROD
136 expanded to surround the karyosome and individual kinetochore foci could no longer be
137 observed. This behavior of the RZZ complex likely corresponds to expansion of the
138 fibrous corona, observed in miotic cells that lack kinetochore-microtubule (KT-MT)
139 attachments [25, 29]. This expansion is thought to facilitate microtubule capture by
140 increasing the surface area of the kinetochore which can contact the microtubules.
141 Thus, in *Drosophila* meiotic oocytes, the fibrous corona expands when microtubules are
142 absent.
143 Activation of the SAC is also associated with elevated Aurora B activity [30]. In
144 *Drosophila* oocytes, the chromosomal passenger complex (CPC) is recruited to the
145 chromosomes but then moves to the central spindle in prometaphase I oocytes [31].
146 CPC proteins are not detected at the meiotic centromeres in fixed samples [31, 32]. In
147 colchicine-treated oocytes, however, the CPC component INCENP localized to the
148 chromosomes and the centromeres (Figure 1B, C). These results suggest that, like
149 MAD1, colchicine treatment causes increased localization of the CPC to the
150 centromeres.

151 ***Effect of kinetochore-microtubule attachments on the SAC***
152 ***response***

153 In all colchicine-treated oocytes, MAD1 localization was consistent and observed
154 on all kinetochores, suggesting a global SAC response to the absence of microtubules.
155 To investigate the mechanism of SAC activation, we examined MAD1 localization in
156 oocytes where end-on attachments or tension was disrupted. NDC80 is required for

157 end-on attachments, so nearly all attachments in *Ndc80*^{RNAi} oocytes are lateral [22].
158 MAD1 was not detected in *Ndc80*^{RNAi} oocytes unless they were treated with colchicine,
159 suggesting that the SAC is insensitive to the loss of end-on attachments (Figure 2A-C).
160 We also examined MAD1 in a *mei-218* mutant (*mei-218*^{null}), which has a high error rate
161 and lacks tension on the kinetochores due to the absence of chiasmata [33]. MAD1 was
162 not detected in *mei-218*^{null} oocytes unless they were treated with colchicine, suggesting
163 that loss of tenson does not induce a SAC response (Figure 2A, B, D). The absence of
164 MAD1 in the untreated *mei-218*^{null} oocytes is consistent with the prior observation that
165 oocytes lacking chiasma bypass the metaphase I arrest and precociously enter
166 anaphase in stage 14 oocytes [33]. These results show that the SAC is only activated in
167 the absence of microtubules and does not respond to the lack of stable attachments,
168 biorientation errors, or tension.

169 *Localization of checkpoint proteins in Drosophila oocytes*
170 *depends on SPC105R*

171 The outer kinetochore protein KNL1/SPC105R is involved in the recruitment of
172 several checkpoint proteins in mitotic cells [34, 35]. Therefore, we investigated the role
173 of SPC105R, the *Drosophila* homolog of KNL1, in the recruitment of MAD1, ROD,
174 MPS1, and the CPC to kinetochores in *Drosophila* oocytes. To test if SPC105R is
175 required for the recruitment of INCENP and MAD1, we treated *Spc105R*^{RNAi} oocytes
176 with colchicine. Colchicine-induced kinetochore localization of both INCENP and MAD1
177 depended on SPC105R (Figure S 2A-D). However, both still localized to the
178 chromosomes. In the absence of SPC105R, MAD1 moved to the pericentric regions
179 adjacent to the centromeres, while INCENP localized to all chromatin and occasionally

180 to regions adjacent to the chromatin. The observation that MAD1 localized in colchicine-
181 treated oocytes depleted of SPC105R suggests that the oocyte can respond to the loss
182 of microtubules even in the absence of the outer kinetochore.

183 We also examined localization of INCENP and MAD1 in *Spc105R* deletion
184 mutants to investigate the domains of SPC105R required for the SAC response (Figure
185 S 3). Because *Spc105R* is an essential gene, we used a combination of $Spc105R^{RNAi}$
186 and RNAi-resistant transgenes to examine mutants in oocytes. The control for each
187 mutant was an RNAi-resistant wild-type transgene, $Spc105R^{B}$ (Figure S 3). MAD1
188 kinetochore localization was reduced in mutants such as $Spc105R^{C}$ or $Spc105R^{\Delta M}$ that
189 deleted motifs (MELT, KI, and ExxEED) in the central region of SPC105R (Figure S 2A,
190 B). INCENP kinetochore localization was also lost from the kinetochore in the majority
191 of $Spc105R^{C}$ or $Spc105R^{\Delta M}$ oocytes, but due to the diffuse chromatin localization, this
192 was not reflected in significant differences in intensity (Figure S 2C, D). These results
193 suggest that the MELT-like, KI-like, and ExxEED repeats are involved in recruiting
194 MAD1 and the CPC to the kinetochore as part of the SAC response.

195 MPS1 localization depends on SPC105R, as shown by its drastic reduction in
196 $Spc105R^{RNAi}$ oocytes (Figure S 4A, B). $Ndc80^{RNAi}$ oocytes also had a decrease in MPS1
197 localization, but this was less severe than $Spc105R^{RNAi}$ oocytes, indicating that the
198 majority of MPS1 is recruited by SPC105R (Figure S 4A, C). Similarly, the $Spc105R^{C}$,
199 $Spc105R^{\Delta M}$, and $Spc105R^{\Delta ExxEED}$ mutants had significant decreases in MPS1
200 localization, but not to the same degree as the $Spc105R^{RNAi}$ oocytes (Figure S 4B, D).
201 Each of these mutants retains the C-terminal domain of SPC105R that recruits NDC80
202 [22]. Thus, these mutants may recruit more MPS1 than $Spc105R^{RNAi}$ oocytes because

203 NDC80 recruits some MPS1. Therefore, these results suggest that MPS1 is recruited by
204 domains within both SPC105R and NDC80.
205 ROD localization also depends on SPC105R, as shown by its reduction in
206 *Spc105R*^{RNAi} oocytes (Figure 3A, B). In comparison to the other SAC proteins,
207 recruitment of RZZ depends on a smaller and specific domain of SPC105R (Figure S 3,
208 Figure 3, D). Oocytes with a deletion of everything except the KT binding domain
209 (*Spc105R*^{C}) or a deletion of all the sequences between the N-terminal and C-terminal
210 domains (MELT-like, KI-like, and ExxEED, termed *Spc105R*$^{\Delta M}$) had almost no ROD^{GFP}
211 localization, similar to *Spc105R*^{RNAi} oocytes. Furthermore, a deletion of the MELT-KI
212 (*Spc105R*$^{\Delta MELT\text{-}KI}$), but not the ExxEED domain, had reduced ROD localization. These
213 results suggest that ROD is recruited by the MELT-KI region. Smaller deletions of only
214 the KI and MELT domains (*Spc105R*$^{\Delta KI}$ and *Spc105R*$^{\Delta MELT}$) resulted in significantly
215 reduced ROD^{GFP} localization at the kinetochores, although these intensities were higher
216 than in the *Spc105R*$^{\Delta MELT\text{-}KI}$ deletion. This suggests that ROD is recruited by both the
217 MELT and KI regions.
218 We also tested if the localization of ROD and MPS1 depended on other SAC
219 proteins. ROD (Figure 4A, B) and MPS1 (Figure 4C, D) localization was significantly
220 reduced in both *Bub3*^{RNAi} and *BubR1*^{RNAi} oocytes. The more significant reductions that
221 were observed with *Bub3* knockdown could be due to less efficient *BubR1*^{RNAi} (see
222 Methods), or redundancy between BUBR1 and BUB1. We also tested the effect of
223 *Cyclin A* knockdown because it may regulate MPS1 localization [36]. *CycA*^{RNAi} oocytes
224 had a significant reduction in MPS1 localization, although not as strong as *Bub3*^{RNAi},
225 and a less significant reduction in ROD localization. Furthermore, MPS1 and ROD

226 localization was inter-dependent, although there was a milder reduction of ROD in
227 *Mps1*^{RNAi}. These results suggest ROD and MPS1 localization depends on both SAC
228 proteins like BUB3 and Cyclin A.

229 ***RZZ and MPS1, but not other SAC proteins, are required for***
230 ***meiosis I biorientation***

231 To determine which SAC genes are required for biorientation during meiosis I,
232 we used fluorescent in-situ hybridization (FISH) probes against the pericentromeric
233 regions of the 2nd, 3rd, and X chromosomes. Biorientation was defined as two
234 homologous centromeres at opposite ends of the karyosome (Figure 5A). A mono-
235 orientation defect was defined as the two homologous centromeres being in the same
236 half of the karyosome. Oocytes from females expressing *rod*^{RNAi} or *Mps1*^{RNAi} had
237 increased chromosome mono-orientation (Figure 5B). The results with *Mps1* are
238 consistent with previous studies showing nondisjunction using fertile allele combinations
239 of *Mps1* [37, 38]. We also tested *CycA*^{RNAi} oocytes, and consistent with a previous
240 report [39], found an elevated level of biorientation defects (Figure 5B).

241 In contrast, *BubR1*^{RNAi}, *Bub1*^{RNAi}*, and Bub3*^{RNAi} oocytes had insignificant
242 frequencies of mono-orientation (Figure 5B). Similarly, we have previously shown that
243 flies with knock down of *Bub1* by RNAi are fertile and do not have increased
244 nondisjunction [31]. BUBR1 is required for sister chromatid cohesion protection in
245 *Drosophila*, however, this may have not been detected by our FISH assay at metaphase
246 I [22, 40]. Mutants of *mad1* and *mad2* are viable and fertile [41, 42], so we used genetic
247 crosses to measure the frequency of nondisjunction (see Methods). Neither mutant had
248 a significant increase in nondisjunction (Table 1). We also used a balancer chromosome

249 to suppress crossing over on the X chromosome (*Bwinscy*), thus testing the role of
250 *mad1* and *mad2* in an achiasmate system [43]. Only a mild increase in nondisjunction
251 was observed. These results suggest that most of the SAC proteins are not required for
252 biorientation of homologous chromosomes at metaphase I, while the RZZ complex and
253 MPS1 may be involved in error correction in addition to their roles in the meiotic SAC.
254 Stage 14 oocytes arrest in metaphase I [33, 44]. If the metaphase I arrest
255 depends on the SAC, we would predict that SAC mutants would precociously bypass
256 this arrest and have increased oocytes with split karyosomes. However, this was not
257 observed in most oocytes, suggesting the metaphase I arrest does not depend on SAC
258 activity (Figure 5C, D). The most striking exceptions were rod^{RNAi} and the *mad2* mutant.
259 The split karyosome phenotype is less than observed in mutants lacking crossing over
260 [22, 33], suggesting these genes could have a minor role in the metaphase I arrest, or in
261 the case of Rod, the precocious anaphase could result from the bi-orientation defects
262 (see below).

263 ***ROD streaming is independent of end-on attachments***

264 MSP1 and ROD may have two distinct functions, one in the SAC and another for
265 biorientation. A striking feature of RZZ is its streaming off the kinetochores, but how
266 streaming contributes to kinetochore attachments and biorientation in meiosis is not
267 known. A small fraction of wild-type oocytes have no ROD streaming, which are likely
268 oocytes in early prometaphase [45]. If streaming is in response to proper attachment of
269 kinetochores to microtubules, we predicted that RZZ would not stream if errors were
270 present, or if end-on attachments could not form. To determine if biorientation errors
271 blocked streaming, we examined ROD in $mei\text{-}218^{null}$ oocytes, in which 90% of

272 crossovers are absent, resulting in frequent chromosome segregation errors [46]. In the
273 absence of crossovers, we still observed precocious anaphase and ROD streaming
274 (Figure 6A,B). Thus, streaming occurs even in the absence of tension and in the
275 presence of attachment errors.

276 To determine if attachment status regulates streaming, we examined ROD in
277 *Ndc80*^{RNAi} oocytes, which lack end-on attachments [21]. Despite the lack of end-on
278 attachments, ROD streamed in all *Ndc80*^{RNAi} oocytes, and there was no effect on ROD
279 accumulation at the kinetochores (Figure 6A-C). Furthermore, oocytes lacking protein
280 phosphatase 2A-B56 (PP2A-B56), which is also required for the creation of end-on
281 attachments [47], still exhibited ROD streaming (Figure 6A-C). Indeed, there may even
282 be a reduction of ROD at the kinetochore in *PP2A-B56*^{RNAi} oocytes. These results
283 demonstrate that end-on attachments are not required for the initiation of RZZ
284 streaming.

285 ***ROD is not required for lateral or end-on attachments***

286 Microtubule nucleation from the kinetochore could depend on RZZ [48]. Thus, the
287 biorientation defects observed in the *rod*^{RNAi} oocytes could be caused by the inability to
288 create lateral or end-on attachments, or the creation of inaccurate attachments. If ROD
289 is necessary for making end-on attachments, we would expect that oocytes depleted of
290 *rod* alone would have lateral attachments. However, most attachments in *rod*^{RNAi}
291 oocytes were end-on (Figure 7A, B). Interestingly, there was an increase of lateral
292 attachments in *rod*^{RNAi} compared to wild-type oocytes. This could be explained if *rod*^{RNAi}
293 oocytes are delayed in making end-on attachments, possibly due to frequent
294 biorientation errors. To test whether ROD was necessary for forming lateral

295 attachments, we knocked down both *rod* and *Ndc80* (*rod*^{RNAi}, *Ndc80*^{RNAi}). Similar to
296 *Ndc80*^{RNAi}, we observed that *rod*^{RNAi}, *Ndc80*^{RNAi} oocytes had primarily lateral
297 attachments, suggesting that ROD is not required for making lateral attachments
298 (Figure 7A, B).

299 As noted above, *rod*^{RNAi} oocytes have an elevated frequency of separated
300 karyosomes. This phenotype was not observed in *rod*^{RNAi}, *Ndc80*^{RNAi} oocytes,
301 suggesting that separated karyosome phenotype is caused by the formation of end-on
302 attachments is required for the (Figure 7A, C).

303 *ROD localization to the kinetochore may delay, but does not*
304 *prevent, end-on attachments*

305 Because ROD is not required for making lateral or end-on attachments, we
306 reasoned that it could be required for regulating the transition from lateral to end-on
307 attachments. This would align with a model proposed in mitotic cells in which high levels
308 of RZZ at the kinetochores inhibit NDC80 from prematurely establishing end-on
309 attachments [23, 24]. In this model, RZZ streaming allows for the establishment of end-
310 on attachments. If this was true in meiosis, we would expect oocytes in which ROD was
311 exclusively on kinetochores and did not stream to have lateral attachments. This ROD
312 behavior was observed in two *Spc105R* mutants. A deletion of the ExxEED repeats
313 (*Spc105R*$^{\Delta ExxEED}$) or the N-terminal region (*Spc105R*$^{\Delta N}$) had higher ROD intensities at
314 the kinetochores (Figure 3) and less streaming than in *Spc105R*^{B} oocytes (Figure 7D,
315 E). However, oocytes with ROD only on kinetochores still exhibited end-on attachments
316 (Figure 7D). These results suggest that the N-terminal region and ExxEED repeats of

317 SPC105R may regulate streaming, and that RZZ streaming is not required for the
318 creation of end-on attachments in *Drosophila* oocytes.
319 To further test whether end-on attachments are inhibited when the RZZ complex
320 is localized to the kinetochore, we stably targeted RZZ to the kinetochore. The rationale
321 for this experiment is that the recruitment of the RZZ components are interdependent
322 [49]. We fused *Zw10* to the KT-binding C-terminal domain of *Spc105R* (*Zw10-*
323 *Spc105R*^{C}), along with three copies of the HA epitope at the C-terminal end (Figure S
324 3). The ZW10-SPC105R^{C} fusion protein was targeted to the kinetochores (Figure 7F).
325 When *Zw10-Spc105R*^{C} was combined with an shRNA targeting the endogenous
326 *Spc105R* (*Spc105R*^{RNAi}), loss of endogenous SPC105R was confirmed cytologically
327 using an antibody against the first 400 amino acids of SPC105R, which is absent in the
328 fusion construct (Figure S 5A). In addition, ROD localized to the kinetochores and did
329 not stream in *Zw10-Spc105R*^{C} oocytes, indicating that the RZZ complex was restricted
330 to the kinetochores (Figure S 5B). ROD^{GFP} did not stream even when there was
331 endogenous SPC105R present at the kinetochores. Thus, the ZW10-SPC105R^{C} fusion
332 protein prevented endogenous RZZ streaming from kinetochores. *Zw10-Spc105R*^{C}
333 oocytes exhibited an increase in lateral attachments compared to *Spc105R*^{C} oocytes
334 (Figure 7G). However, the majority of attachments were still end-on (~60%), indicating
335 that RZZ may delay, but does not prevent, end-on attachments. Therefore, in
336 agreement with the two *Spc105R* mutants (Figure 7D), streaming of RZZ is not required
337 to establish end-on attachments in *Drosophila* oocytes. Indeed, end-on attachments
338 occur while RZZ is localized to the kinetochore.

339 ***Spindly regulates ROD streaming***

340 Streaming is proposed to be dependent on the microtubule motor protein Dynein
341 [50]. To further examine the role of RZZ streaming and the interaction with Dynein in
342 meiosis, we investigated two dynein-associated proteins previously implicated in RZZ
343 removal from the *Drosophila* kinetochores: Spindly [51], and NudE [52]. We performed
344 FISH on stage 14 oocytes to determine whether these two genes are required for
345 chromosome biorientation (Figure 8A, B). There was only a slight increase in
346 chromosome mono-orientation in *nudE*^{RNAi} oocytes compared to wild-type (9% and 0%,
347 respectively). However, 35% of chromosomes were mono-oriented in *Spindly*^{RNAi}
348 oocytes, suggesting that Spindly is necessary for accurate meiotic chromosome
349 segregation.

350 To determine whether these proteins regulate streaming, we characterized ROD
351 behavior in oocytes depleted of *Spindly* or *nudE* (Figure 8C-E). Both *Spindly*^{RNAi} and
352 *nudE*^{RNAi} oocytes exhibited ROD streaming (Figure 8D). This was surprising for Spindly,
353 which has been shown to be required for streaming in *Drosophila* S2 cells [51].
354 However, *Spindly*^{RNAi} oocytes also exhibited unusual behavior, notably ROD streaming
355 in the central spindle region between homologous centromeres in approximately 50% of
356 oocytes (Figure 8E, Figure S 6A). Thus, Spindly may be required for proper streaming
357 towards the spindle pole. To confirm that ROD was being efficiently removed and not
358 accumulating at the kinetochores, we measured the intensity of ROD in *Spindly*^{RNAi} and
359 *nudE*^{RNAi} oocytes (Figure 8F). Both RNAi oocytes had ROD levels similar to those in
360 wild-type oocytes, indicating that ROD can still stream from kinetochores without NudE

361 or Spindly. Therefore, while neither protein is required for RZZ streaming, Spindly may
362 be required for RZZ to stream towards the spindle poles.
363 RZZ is proposed to recruit Spindly to the kinetochore, which is followed by
364 streaming of both Spindly and RZZ [51, 53]. To examine the localization of Spindly on
365 the meiotic spindle, we used previously described *Spindly-GFP* fusion transgenes [54].
366 Oocytes expressing wild-type *Spindly* had weak localization throughout the spindle
367 (Figure S 6B). We also examined *Spindly* mutants with deletions of domains implicated
368 in streaming: the N-terminus (a deletion of amino acids 1-228) and the Spindly Box (a
369 deletion of amino acids 229-250). Both mutants had a dominant sterility phenotype
370 when expressed in oocytes using *matα*, suggesting that these mutants interfere with the
371 activity of the wild-type Spindly protein. In contrast to the wild-type oocytes, which had
372 weak localization throughout the spindle, both mutants had pronounced localization
373 near the centromeres. Spindly$^{\Delta N}$ localized to the kinetochores and spindle, while
374 Spindly$^{\Delta SB}$ primarily localized to the kinetochores (Figure S 6B, C). These results
375 suggest that the Spindly Box domain is important for removal of Spindly from the
376 kinetochores. The robust localization of these mutants was then used to test if ROD is
377 required for Spindly localization, as shown in mitotic cells [51]. Indeed, Spindly was
378 absent in *rod*^{RNAi} oocytes, indicating ROD is required for Spindly localization in oocyte
379 meiosis (Figure S 6C, D).

380

381 # Discussion

382 ### *The function of the SAC in oocytes*

383 We analyzed the localization and meiotic phenotypes of several SAC proteins in
384 *Drosophila* oocytes. Increased localization of MAD1, BUBR1, INCENP, and ROD at the
385 kinetochores following loss of microtubules indicated *Drosophila* oocytes have a
386 functioning SAC. This SAC response was observed even in the absence of a
387 kinetochore. However, a SAC response was not observed following loss of microtubule
388 attachments to the kinetochores, the lack of tension, or the presence of multiple
389 biorientation errors. Thus, the function of the SAC in oocytes may be to promote spindle
390 assembly, rather than proper microtubules attachments to kinetochores [28].

391 Only two of the SAC proteins we tested were required for biorientation of
392 homologous chromosomes at meiosis I, MPS1 [37, 38] and ROD, suggesting that the
393 SAC is not required for error correction. Similarly, *C. elegans* may correct attachment
394 errors using a mechanism that does not rely on the SAC [55]. The SAC may have a
395 more prominent role in chromosome segregation in mouse oocytes that arrest in
396 meiosis II, where increased aneuploidy has been observed with loss of SAC proteins
397 [56, 57]. However, the evidence comes from a variety of assays that may not be
398 comparable to our FISH experiments, and one study concluded that Mad2 is
399 dispensable for accurate meiotic chromosome segregation except in response to stress
400 [58].

401 In most cases, the loss of SAC proteins in *Drosophila* oocytes does not result in
402 progression into anaphase (Figure 5) or a rise in APC activity [59]. These observations
403 suggest the SAC may not regulate the APC in metaphase I-arrested oocytes. Instead,

404 the metaphase I arrest in *Drosophila* oocytes may be maintained by a SAC-independent
405 mechanism relying on chiasmata and cohesion, with progression into anaphase I
406 depending on cohesion release. This would explain why *Drosophila* oocytes lacking
407 chiasmata and tension bypass metaphase I arrest and progress into anaphase I [33,
408 60].

409 Furthermore, several observations suggest that the SAC is silenced in oocytes,
410 possibly to allow for developmental regulation of the metaphase I arrest, with
411 progression into anaphase occurring only after oocytes enter the oviduct.
412 Developmentally regulated SAC silencing would explain why ROD streams in wild-type
413 metaphase I-arrested oocytes, even in the absence of end-on attachments or the
414 presence of multiple biorientation errors in *Ndc80*^{RNAi} and *PP2A-B56*^{RNAi} oocytes [61].
415 Similarly, MAD2 localizes to centromeres in early (stage 13) but not late (stage 14)
416 stage oocytes [45], and the metaphase I spindle has some anaphase-like
417 characteristics such as high concentrations of the CPC on the central spindle [62].
418 Yeast meiotic cells silence their SAC to prevent prolonged arrest, indicating this may be
419 a conserved feature of meiotic cells [63].

420 ***Recruitment of checkpoint proteins during meiosis***

421 Our results are consistent with the known role of KNL1/SPC105R in the
422 recruitment of checkpoint proteins to the kinetochore [1]. We previously showed that
423 BUBR1 is recruited by both the MELT-KI and C-terminal regions of SPC105R [22].
424 MAD1, INCENP, and probably BUB3 depend on the MELT-KI and ExxEED repeat
425 regions of SPC105R, which correspond to the repeated MELT motifs found in
426 vertebrate KNL1. In the absence of SPC105R, recruitment of MAD1 shifts to the peri-

427 centromeric regions. Thus, some components of the SAC do not depend on SPC105R,
428 and there is a SPC105R-independnet SAC response. Human cells may also have two
429 SAC pathways, and one is active in the absence of KNL1 [64]. Thus, centromere
430 components may recruit SAC proteins. In *Drosophila*, this could be facilitated by ZW10,
431 which interacts with and is recruited by centromere protein CAL1 [65].

432 ***Multiple functions and recruitment factors for MPS1 and RZZ***

433 MPS1 was originally discovered with the mutation *ald* as being required for
434 meiotic chromosome segregation [66], and subsequent studies have characterized its
435 role in *Drosophila* meiosis [37, 38] and mouse oocytes [67]. While MPS1 has been
436 shown to be recruited by NDC80 [68-71], two observations show that a significant
437 amount of MPS1 is also recruited by SPC105R. First, we observed a more severe
438 decrease in MPS1 localization upon *Spc105R* depletion than *Ndc80* depletion. Second,
439 we observed a decrease in MPS1 localization in *Spc105R* mutants that still recruit
440 NDC80. These data suggest that MPS1 is recruited by both NDC80 and SPC105R in
441 *Drosophila* oocytes. The SPC105R-dependent MPS1 could function in the SAC while
442 NDC80-dependent MPS1 could regulate attachments [68, 72].

443 Like MPS1, the RZZ complex has roles in error correction and in the SAC. Like
444 MPS1, our data suggest there are two separate RZZ populations: one that is recruited
445 by BUB3 and BUBR1 and is involved in the SAC and a second that is recruited by the
446 MELT-KI domains of SPC105R and is important for EC. The SAC population of ROD
447 that depends on BUB3 could recruit other checkpoint proteins like MAD1 and MAD2
448 [73, 74]. These conclusions are based on the observation that unlike rod^{RNAi}, $Bub3^{RNAi}$
449 and $BubR1^{RNAi}$ oocytes do not have biorientation defects, suggesting that BUB3 and

450 BUBR1 do not recruit the population of RZZ which is involved in error correction.
451 Furthermore, there is a substantial amount of ROD^{GFP} remaining after *Bub3* and *BubR1*
452 are knocked down, arguing that they do not recruit the total population of RZZ at
453 kinetochores. However, the *Spc105R*$^{\Delta MELT\text{-}KI}$ mutant (deleting amino acids 154-840)
454 abolishes nearly all ROD^{GFP} localization and does have biorientation defects [22].
455 Therefore, the MELT-KI domains of SPC105R are likely involved in recruiting the
456 populations of RZZ involved in EC, independently of BUB3.
457 The MELT-KI region of SPC105R is highly conserved [75]. Indeed, our results
458 refine observations made in HeLa cells showing that the N-terminal domain of KNL1
459 recruits RZZ [76, 77]. In *Drosophila* cell lines, a region within the KI-like domain (amino
460 acids 266-384) and BUBR1 are required for RZZ recruitment to kinetochores [78].
461 Interestingly, this study also showed that the recruitment of RZZ by SPC105R could
462 promote chromosome movement towards the spindle poles. Like this study, we found
463 the KI domain recruits the majority of RZZ. It remains to be determined, however, why
464 both the MELT and KI domains are required to recruit RZZ and for biorientation in
465 meiosis I [22].
466 ROD and MPS1 localization was reduced in *CycA*^{RNAi} oocytes, and *CycA*^{RNAi}
467 oocytes have biorientation defects in *Drosophila* oocytes [39]. Indeed, Cyclin A has
468 been shown to regulate KT-MT attachments in mammalian cells [79, 80] and in
469 *Drosophila* in mitotic cells, Cyclin A/CDK1 activates Polo kinase, which has recently
470 been shown to regulate Spindly and prevent it from inhibiting RZZ [24]. One explanation
471 for these results is that Cyclin A is required for the functions of ROD and MPS1
472 associated with ensuring the accuracy of biorientation.

473 ***The role of RZZ localization in attachment stabilization***

474 Previous studies in *C. elegans, Drosophila,* and human mitotic cells have
475 suggested a two-part model for how RZZ regulates KT-MT attachments [23, 24, 81, 82].
476 First, RZZ interacts with NDC80 to inhibit end-on attachments. Second, Spindly-
477 dependent RZZ streaming alleviates RZZ inhibition to allow for the formation of end-on
478 attachments. Three of our observations are consistent with this hypothesis. First,
479 knockdown of *Spindly* resulted in a decrease in end-on and an increase in lateral
480 attachments. This would be expected if Spindly negatively regulates RZZ. Second,
481 *Zw10* fused to the C terminus of *Spc105R* led to complete RZZ retention on the
482 kinetochores and increased lateral attachments. Third, we observed an increase in
483 karyosome separation in rod^{RNAi} oocytes, which could be due to precocious stabilization
484 of end-on attachments [22, 83]. These results suggest that the RZZ complex at the
485 kinetochore has a role in preventing or delaying end-on attachments.

486 However, some of our results are not consistent with this model. Oocytes
487 expressing $Zw10\text{-}Spc105R^{C}$ primarily had end-on attachments. A similar observation
488 was made with two mutants ($Spc105R^{\Delta ExxEED}$ and $Spc105R^{\Delta N}$) that had reduced ROD
489 streaming but still formed end-on attachments. Therefore, if KT-localized RZZ inhibits
490 end-on attachments, this can be overridden in oocytes. Finally, ROD streaming was
491 observed in the absence of end-on attachments. Thus, physical removal of RZZ (or
492 streaming) may not be required for the formation of end-on microtubule attachments,
493 and alternative mechanisms for regulating this population of RZZ may exist. For
494 example, a conformational change in RZZ may affect its regulation of attachments [23].
495 Understanding the relationship between the localization of the RZZ complex and its

496 effects on microtubule attachments is crucial for analyzing its role in promoting accurate
497 chromosome segregation during female meiosis.

498 ***The role of Spindly in meiotic RZZ streaming and homolog***
499 ***biorientation***

500 Spindly has a conserved role as a Dynein adaptor [84], and we have shown that
501 RZZ recruits Spindly to kinetochores in *Drosophila* oocytes. Spindly has been shown in
502 multiple organisms to recruit Dynein, resulting in removal of the RZZ complex from the
503 kinetochores to stabilize microtubule attachments [24, 53, 81, 85]. This activity has been
504 used to explain why depletion of RZZ can suppress defects in mitotic cells depleted of
505 Spindly [23, 24, 81]. However, the role of Spindly in meiosis has not been reported.
506 Spindly is required for biorientation of homologous chromosomes during oocyte
507 meiosis. The failure to remove RZZ from the kinetochores could be the reason for the
508 meiotic biorientation defect. Contrary to the expectations from data in mitotic cells
509 described above, however, knocking down *Spindly* did not abolish ROD streaming.
510 Instead, we found that ROD displayed abnormal behaviors in oocytes depleted of
511 *Spindly*, such as streaming in the opposite direction and localizing in the central spindle
512 region between kinetochores. Therefore, it is likely that other proteins are involved in the
513 removal of RZZ from the kinetochores in oocytes.
514 In the absence of Spindly in HeLa cells, alternative mechanisms are activated to
515 remove kinetochore proteins [86]. One candidate is CENP-E, which is a plus-end
516 directed motor required for the fibrous corona [87], and is required for homolog
517 biorientation in *Drosophila* oocytes [21]. Given that RZZ can move SPC105R oligomers
518 [88], and our observation that streaming off the kinetochore may not affect attachment

519 status, an important role of RZZ may be to move kinetochores. Rather than being
520 necessary for the direct removal of RZZ from the kinetochores, Spindly, CENP-E, and
521 RZZ might form a complex capable of bidirectional movement of the kinetochores [89].
522 Understanding how RZZ regulates biorientation may depend on reconciling the relative
523 importance of two activities, RZZ moving kinetochores with motors like Dynein and
524 CENP-E, and RZZ blocking or delaying end-on attachments.

525

526 # Materials and Methods

527 ## *Drosophila Genotypes and Expression of Transgenes and*

528 ## *shRNAs*

529 The transgenes and mutants used in this study are listed in Table 2. The
530 localization of SAC proteins was examined in *Drosophila* oocytes using GFP fusion
531 transgenes, most under the control of their own promoter. To examine MPS1, we used
532 a construct used extensively in cell culture but modified for making transgenics
533 (*P{EGFP-Mps1.F}* = $Mps1^{GFP}$) [90, 91]. To visualize the RZZ complex in oocytes, we
534 used a construct where ROD was tagged with Green Fluorescent Protein (GFP) at the
535 N-terminus and under the control of its own promoter (*P{gEGFP-rod}* = rod^{GFP}) [25]
536 (Figure S 1A). Expression of either transgene resulted in very low levels (~0.25%) of X-
537 chromosome nondisjunction (Table S1), which was comparable to wild-type strains [92].
538 This is consistent with previous studies showing that this transgene can rescue the
539 lethality of *rod* mutants [25, 93].

540 The UAS/GAL4 system was utilized to drive expression of many of the
541 transgenes in oocytes. *Matα* was used to induce expression following DNA replication
542 and early pachytene and throughout meiotic prophase.

543 A fusion between the C-terminal domain of *Spc105R* and the entire coding region
544 of Z*w10* was generated by GenScript in pENTR4. The C-terminal fragment of SPC105R
545 has been characterized previously and is sufficient for kinetochore localization [22]. The
546 fusion gene was transferred into pPWH, which fused the coding region to a 3XHA tag at

547 the C-terminal end. This was injected into embryos for germline transformation by
548 Model Systems Injections.

549 ### *RNA Extraction and Quantification of RNAi Knockdown*

550 Among three shRNA lines targeting *rod*, one (*P{Val22:rod-153}1attP40,* =
551 $rod^{RNAi)}$) was chosen because it had the strongest phenotype and most severe mRNA
552 knockdown (4% of the wild-type). Expression of rod^{RNAi} using *matα* produced sterile
553 females and ubiquitous expression caused lethality. To confirm the efficacy of the
554 rod^{RNAi} in oocytes, we examined ROD^{GFP} in oocytes expressing the *rod* shRNA. The
555 intensity of ROD^{GFP} at the kinetochores in rod^{RNAi} oocytes was reduced to nearly
556 background levels (Figure S 1B, C), indicating that the *rod* shRNA provides a strong
557 knockdown of *rod*. Similarly, the intensity of $MPS1^{GFP}$ at the kinetochores in $Mps1^{RNAi}$
558 oocytes was significantly reduced (Figure S 1D, E).

559 RT-qPCR was performed to determine knockdown of mRNAs for each shRNA.
560 After the parental flies were crossed, mature female offspring with the correct genotype
561 were collected into yeasted vials for three days. These flies were then ground in 1X
562 phosphate-buffered saline (PBS) and filtered through meshes to isolate the stage 14
563 oocytes. 1 mL of TRIzol reagent was added and RNA was extracted per the
564 manufacturer's instructions (Thermo Fisher Scientific). Taqman RT-qPCR was
565 performed to quantify RNAi knockdowns. 2 µg of isolated RNA was reverse transcribed
566 into cDNA using the High Capacity cDNA Reverse Transcription Kit (Applied
567 Biosystems). Afterwards, qPCR was performed using a TaqMan Assay (Thermo
568 Scientific) with four replicates per reaction. The efficacy of RNAi knockdowns has been
569 published for *Ndc80 GL00625* = 6% remaining*, Spc105R GL00392* = 13% remaining

570 [21], *Bub1 GL00151* = 2% remaining [31], *BubR1 GLV21065* = 22% remaining, *BubR1*
571 *GL00236*= 27% remaining, and *Bub3 HMS00789* = 0.7% remaining.

572 ### *Measuring X-Chromosome Nondisjunction*

573 To measure nondisjunction of the X chromosome, virgin females with the desired
574 genotype were crossed to males with a dominant *Bar* mutation on the Y chromosome
575 (*yw/B^{S}Y*). This mutation led to a visible bar-eyed phenotype where the eye was thinner
576 than wild-type eyes. The normal segregation of chromosomes would lead to female
577 offspring (XX) with wild-type eyes and males (XY) with bar eyes. If a nondisjunction
578 event occurred in the X chromosome, the following sex chromosome combinations were
579 possible: XO, XXY, XXX, and YO. XO and XXY were viable and resulted in normal-eyed
580 males and bar-eyed females, respectively. XXX and YO were lethal. To calculate
581 nondisjunction rates while taking into account the lethal genotypes, the following
582 equation was used: $\frac{\#\ flies\ with\ nondisjunction \times 2}{(\#\ flies\ with\ nondisjunction \times 2) + (\#\ of\ normal\ flies)}$. This rate determined
583 whether a particular genotype resulted in increased meiotic nondisjunction.

584 ### *Cytology of Stage 14 Oocytes*

585 Cytology of stage 14 oocytes was performed as previously described [94]. After
586 the parental flies were crossed, mature female offspring with the correct genotypes
587 were collected into yeasted vials for one to two days. These flies were then broken open
588 in a blender while in 1x modified Robb's buffer and filtered through meshes to isolate
589 the stage 14 oocytes. If a colchicine treatment was needed, oocytes were incubated
590 with 150 μM colchicine or 0.5% EtOH in modified Robb's buffer for one hour to remove
591 all microtubules. The oocytes were fixed with 5% formaldehyde and heptane before

592 being rinsed in 1X PBS. The oocytes were then rolled between the frosted surface of a
593 glass slide and a cover slip to remove the membranes and nutated for two hours in
594 PBS/1% Triton X-100 to make them permeable to antibody staining. Afterwards,
595 oocytes were washed in PBS/0.05% Triton X-100 and blocked for one hour in blocking
596 buffer (0.5% BSA and 0.1% Tween-20 in 1X PBS). Subsequently, primary antibodies
597 were added to the oocytes while the secondary antibodies were added to *Drosophila*
598 embryos to remove any nonspecific binding. After nutating overnight at 4°C, the oocytes
599 were washed in blocking buffer four times at room temperature for 15 minutes. The
600 secondary antibodies were added and the oocytes were nutated for 3-4 hours at room
601 temperature. The oocytes were then washed in blocking buffer with Hoechst33342 (10
602 μg/mL) to stain the DNA. The oocytes were washed twice more in blocking buffer and
603 then were ready for mounting and imaging.

604 The primary antibodies used in this paper were tubulin monoclonal antibody
605 DM1A at 1:50 conjugated to FITC (Sigma-Aldrich), tubulin E7 monoclonal antibody at
606 1:150 [95], rat anti-INCENP at 1:600 [96], guinea pig anti-CENP-C at 1:1000 [97], rat
607 anti-tubulin at 1:300 (Millipore), rabbit anti-Spc105R (1:4000) [98], rabbit anti-GFP
608 (1:200) (Thermo Fisher), rat anti-HA (Roche, 1:50). Multiply preabsorbed secondary
609 antibodies were from Jackson ImmunoResearch, and were conjugated to Alexa 647,
610 Cy3, Alexa 594 or Alexa 488.

611 To visualize pairs of homologous chromosomes, fluorescent *in situ* hybridization
612 (FISH) was performed. After oocytes fixation, 2X SSC was added and the membranes
613 were removed by rolling the oocytes between glass slides. The oocytes were then
614 nutated in increasing concentrations of formamide solution (20%, 40%, and 50%) before

615 being added to the hybridization solution and probes. The probes were synthesized by
616 IDT, and recognize the 359 bp repeats on the X chromosome (labeled with AlexaFluor
617 594), the AACAC repeats on the second chromosome (labeled with Cy3), or the dodeca
618 repeats on the third chromosome (labeled with Alexa 647). This was followed by
619 incubation in 80°C for 20 minutes and then 37°C overnight. The next day, the oocytes
620 were washed in 50% formamide solution twice at 37°C and 20% formamide once at
621 room temperature. The oocytes were then rinsed three times in 2X SSCT, once in 2X
622 PBST, and nutated in blocking buffer for 4 hours at room temperature. Afterwards,
623 mouse anti-tubulin-FITC antibody (Sigma) was added (1:50) and the oocytes were
624 nutated overnight at room temperature. The next day, the oocytes were washed in
625 blocking buffer with Hoechst33342 (10 µg/mL). After washing twice more with blocking
626 buffer, the oocytes were mounted and imaged.

627 ***Imaging Oocytes, Image Analysis, and Statistical Analysis***

628 Oocytes were mounted on a glass slide in SlowFade Gold (Invitrogen) and
629 images were taken with a 63x lens on a Leica SP8 or Stellaris microscope. Protein
630 intensities were quantified using Imaris image analysis software (Bitplane). To measure
631 the intensity of proteins at kinetochores, spots marking the kinetochores and random
632 areas of the background were created. The average intensity of the protein of interest at
633 the background was subtracted from the intensity at each kinetochore to generate the
634 normalized intensity value. GraphPad Prism software was used to graph data and
635 perform statistical analysis. All statistical tests and sample sizes are reported in the
636 figure legends.
637

638 ***Data availability statement***

639 All the data underlying this study are available in the published article and its
640 online supplementary material.

641

642 ***Acknowledgements***

643 We thank Marina Druzhinina for technical assistance, Christian Lehner, and
644 Rager Karess for providing Drosophila stocks and antibodies. Stocks obtained from the
645 Bloomington Drosophila Stock Center (NIH P40OD018537) were used in this study. The
646 E7 tubulin monoclonal antibody was obtained from the Developmental Studies
647 Hybridoma Bank, created by the NICHD of the NIH and maintained at The University of
648 Iowa, Department of Biology, Iowa City, IA 52242. Image acquisition and analysis was
649 made possible by the Waksman Institute Shared Imaging Core Facility and The Human
650 Genetics Institute Imaging Core Facility at Rutgers. This work was supported by NIH
651 grant GM101955 to K.S.M.

652

653

654

655 Table 1: Nondisjunction in *mad* mutants

656

Genotype	XX	XY	XXY	XO	% NDJ
mad2^{EY21687}*/Df*	3857	3558	6	17	0.6
mad1^{1}*/Df*	805	769	1	6	1.0
Bwinscy/+; mad2^{EY21687}*/Df*	357	263	4	12	4.9
Bwinscy/+; mad1^{1}*/mad1*^{1}	427	321	9	4	3.4
Bwinscy/+; mad1^{1}*/+*	588	375	2	4	1.2
Bwinscy/+; mad2^{EY21687}*/+*	509	301	2	2	1.0

657 *mad2* Df = *Df(3L)Exel6107* and *mad1* Df = *Df(2R)ED1791*

658

659

660

661

662 Table 2. *Drosophila* genotypes used in this work.

Genotype	Abbreviation	Reference
P{w^{+mC}=matalpha-GAL-VP16}V37	*matα*	[99]
P{Val22:rod-153}attP40	*rod^{RNAi}*	This paper
P{gEGFP-rod}	*rod^{GFP}*	[25]
P{EGFP-Mps1.F}	*Mps1^{GFP}*	[90]
P{Mad1-GFP}	*Mad1^{GFP}*	[42]
P{BubR1.GFP}	*BubR1^{GFP}*	[73]
P{gEGFP-Bub3}III.3	*Bub3^{GFP}*	[100]
P{w^{+mC}=UASp-Spc105RB}	*Spc105R^{B}*	[22]
P{UASp-Spindly.RR.GFP}	*Spindly^{GFP}*	[54]
P{w^{+mC}=UASp-Zw10-Spc105RC}	*Zw10-Spc105R^{C}*	This paper
P{TRiP.GL00392}attP2	*Spc105R^{RNAi}*	[101]
P{TRiP.GL00625}attP40	*Ndc80^{RNAi}*	[101]
P{TRiP.HMS01283}attP2	*Spindly^{RNAi}*	[101]
P{TRiP.HMS01868}attP40	*nudE^{RNAi}*	[101]
P{TRiP.GL00151}attP2	*Bub1^{RNAi}*	[101]
P{wrd^{GL00671}wdb^{HMS01864}}/TM3	*PP2A-B56^{RNAi}*	[101]
P{TRiP.GL00236}attP2	*BubR1^{RNAi}*	[101]
P{TRiP.HMS00789}attP2	*Bub3^{RNAi}*	[101]
Mad1^{1}	*Mad1*	[42]

Mad2^{EY21687}	*mad2*	[41]
mei-218^{6}	*mei-218*^{null}	[102]
Mps1^{ald}	*Mps1*^{ald}	[66]
Mps1^{C3}	*Mps1*^{C3}	[37]

663
664

665

Figure Legends

Figure 1. **Localization of SAC proteins in oocytes**.

(A, B) Oocytes were incubated for one hour in Robb's buffer with 0.5% EtOH (A) or 250 µM colchicine (B). BUBR1, BUB3, MPS1, ROD, and MAD1 were detected using GFP-tagged transgenes, while INCENP was detected using an anti-INCENP antibody (all proteins shown in green), DNA is in blue, CENP-C in white, and tubulin in red. Single channel images show SAC protein localization. All images are maximum intensity projections of z stacks. Scale bars represent 5 µm. (C) Quantification of SAC protein intensity at kinetochores, normalized to background signal (n for EtOH and colchicine = 313 and 174 for BUBR1, 67 and 83 for BUB3, 219 and 356 for MPS1, 139 and 184 for ROD, 138 and 185 for MAD1, and 74 and 200 for INCENP). Error bars show mean ± s.d.; ****P<0.0001, ns=no significance (unpaired two-tailed t test).

Figure 2. **Induction of MAD1 localization is independent of tension and attachment status**.

(A, B) MAD1^{GFP} localization in wild-type, *Ndc80*^{RNAi}, or *mei-218*^{null} oocytes that were either untreated (A) or treated with 250 µM colchicine (B). MAD1^{GFP} is shown in green, DNA in blue, CENP-C in white, and tubulin in red. Single channel images (bottom) show MAD1^{GFP} with karyosome outlines in dashed blue in (A). All images are maximum intensity projections of z stacks. Scale bars represent 5 µm. (C, D) Quantification of MAD1^{GFP} intensity at kinetochores, normalized to background GFP signal (n =106 and 127 kinetochores for (C) and 158 and 311 kinetochores for (D)). Error bars show mean ± s.d.; ****P<0.0001 (unpaired two-tailed t test).

Figure 3. **ROD localization depends on the MELT-KI domain of SPC105R**.

(A) ROD^{GFP} localization in control and an *Spc105R*^{RNAi} oocytes, with ROD^{GFP} in green, DNA in blue, CENP-C in white, and tubulin in red. Single channel images (bottom) show ROD^{GFP}. (B) Quantification of ROD^{GFP} intensity at kinetochores normalized to background GFP signal in indicated oocytes (from left to right, n = 142, 169, 144, 144, 167, 138, 206, 159, 173, and 146 kinetochores). Error bars show mean ± s.d.; ****P<0.0001, ***P=0.0006, ns=no significance (unpaired two-tailed t test). All *Spc105R* mutants are in an *Spc105R*^{RNAi} background targeting the endogenous *Spc105R*. (C) Schematic of SPC105R^{B} domains in *Drosophila melanogaster*. (D) ROD^{GFP} localization in the indicated *Spc105R* mutant oocytes, with ROD^{GFP} in green, DNA in blue, CENP-C in white, and tubulin in red. Single channel images (bottom) show ROD^{GFP}. All images are maximum intensity projections of z stacks. Scale bars represent 5 µm.

Figure 4. **ROD and MPS1 localization depend on SAC genes**.

704 (A) ROD^{GFP} localization in wild-type, *Bub3*^{RNAi}, *BubR1*^{RNAi}, *Mps1*^{RNAi}, and *CycA*^{RNAi}
705 oocytes with ROD^{GFP} in green, DNA in blue, CENP-C in white, and tubulin in red. Single
706 channel images (bottom) show ROD^{GFP}. (B) Quantification of ROD^{GFP} intensity at
707 kinetochores, normalized to background GFP signal in indicated oocytes (from left to
708 right, n = 142, 170, 66, 76, and 155 kinetochores). Error bars show mean ± s.d.;
709 ****P<0.0001, *P≤0.0123 (unpaired two-tailed t test). (C) MPS1^{GFP} localization in wild-
710 type, *Bub3*^{RNAi}, *BubR1*^{RNAi}, *rod*^{RNAi}, and *CycA*^{RNAi} oocytes with MPS1^{GFP} in green, DNA
711 in blue, CENP-C in white, and tubulin in red. Single channel images (bottom) show
712 MPS1^{GFP}. (D) Quantification of MPS1^{GFP} intensity at kinetochores, normalized to
713 background GFP signal in indicated oocytes (from left to right, n = 455, 97, 149, 180,
714 and 152 kinetochores). Error bars show mean ± s.d.; ****P<0.0001 (unpaired two-tailed
715 t test). All images are maximum intensity projections of z stacks. Scale bars represent 5
716 µm.
717

718 Figure 5. **Meiotic chromosome alignment in SAC RNAi oocytes**.

719 (A) Representative images depicting chromosome orientation in wild-type, *rod*^{RNAi}, and
720 *Mps1*^{RNAi} oocytes. Images show DNA (blue), tubulin (green), the X chromosome
721 (magenta), the second chromosome (red), and the third chromosome (white). Tubulin
722 and FISH probes are also shown in a separate channel, with examples of mono-
723 oriented chromosomes circled. All images are maximum intensity projections of z
724 stacks. Scale bars represent 5 µm. (B) Percent of chromosomes per oocyte with the
725 indicated orientation (from left to right, n = 132, 65, 114, 94, 65, 66, 87, 39, and 30 pairs
726 of chromosomes). ****P<0.0001 (Fisher's exact test). (C) Examples of wild-type, *mad1*^{1},
727 and *mad2*^{EY21687} mutant oocytes, with tubulin in green, DNA in blue, CENP-C in red, and
728 INCENP in white. Single channel images show DNA. (D) Percent of oocytes with the
729 specified karyosome morphology (from left to right, n=114, 102, 103, 41, 31, 32, and 31
730 oocytes). **P=0.0020, *P=0.0375 (Fisher's exact test).
731

732 Figure 6. **ROD streams in the absence of tension and end-on attachments**.

733 (A) ROD^{GFP} localization in wild-type, *mei-218*^{null}, *Ndc80*^{RNAi}, and *PP2A-B56*^{RNAi} oocytes
734 with ROD^{GFP} in green, DNA in blue, CENP-C in white, and tubulin in red. Single channel
735 images (bottom) show ROD^{GFP}. All images are maximum intensity projections of z
736 stacks. Scale bars represent 5 µm. (B) Percent of oocytes with ROD^{GFP} streaming in
737 indicated genotypes (from left to right, n = 25, 15, 22, and 16 oocytes), ns=no
738 significance (Fisher's exact test). (C) Quantification of ROD^{GFP} intensity at kinetochores,
739 normalized to background GFP signal in indicated oocytes (from left to right, n = 142,
740 139, and 92 kinetochores). Error bars show mean ± s.d.; *P=0.0202 (unpaired two-tailed
741 t test).
742

743 Figure 7. **ROD is not required for microtubule attachments**.

744 (A) Wild-type; *rod*^{RNAi}; *Ndc80*^{RNAi}; and *rod*^{RNAi}, *Ndc80*^{RNAi} oocytes with tubulin in green,
745 DNA in blue, CENP-C in white, and INCENP in red. *Rod*^{RNAi} oocyte on the left has an
746 intact karyosome and on the right a split karyosome. (B) Percent of kinetochores per
747 oocyte with lateral kinetochore-microtubule attachments in indicated genotypes (from
748 left to right, n = 40, 46, 30, 20, and 31 oocytes). Error bars show s.d.; ****P<0.0001,
749 ***P=0.0007, ns=no significance (unpaired two-tailed t test). (C) Percent of oocytes with
750 the specified karyosome morphology in the indicated genotypes (from left to right, n =
751 41, 46, 22, 20, and 31 oocytes). ***P=0.0002, *P=0.0260 (Fisher's exact test). (D)
752 ROD^{GFP} localization in *Spc105R*^{B}, *Spc105R*$^{\Delta N}$, and *Spc105R*$^{\Delta ExxEED}$ oocytes with
753 ROD^{GFP} in green, DNA in blue, CENP-C in white, and tubulin in red. Single channel
754 images (bottom) show ROD^{GFP}. All *Spc105R* mutants are in an *Spc105R*^{RNAi}
755 background targeting the endogenous *Spc105R*. (E) Percent of oocytes with ROD^{GFP}
756 streaming in indicated genotypes (from left to right, n = 25, 20, 20, and 28 oocytes);
757 **P=0.0012 (Fisher's exact test). (F) *Spc105R*^{C} and *Zw10-Spc105R*^{C} oocytes (both in
758 an *Spc105R*^{RNAi} background) with DNA in blue, CENP-C in white, tubulin in red, and
759 ZW10-SPC105R^{C} in red (right). Single channel images (bottom) show CENP-C (left) or
760 ZW10-SPC105R^{C} (right). (G) Percent of kinetochores per oocyte with lateral
761 kinetochore-microtubule attachments in indicated genotypes (n = 42 and 51 oocytes).
762 Error bars show s.d.; ****P<0.0001 (unpaired two-tailed t test). All *Spc105R*^{C} and *Zw10-*
763 *Spc105R*^{C} oocytes are in an *Spc105R*^{RNAi} background targeting the endogenous
764 *Spc105R*. All images are maximum intensity projections of z stacks. Scale bars
765 represent 5 µm.
766

767 Figure 8. **Requirement for Spindly in meiosis and interactions with ROD.**

768 (A) Representative images depicting chromosome orientation in wild-type, *Spindly*^{RNAi},
769 and *nudE*^{RNAi} oocytes. Images show DNA (blue), tubulin (green), the X chromosome
770 (magenta), the second chromosome (red), and the third chromosome (white). Tubulin
771 and FISH probes are also shown in a separate channel, with examples of mono-
772 oriented chromosomes circled. (B) Percent of chromosomes per oocyte with the
773 indicated orientation (from left to right, n = 86, 66, and 54 pairs of chromosomes);
774 ****P<0.0001, **P=0.0076 (Fisher's exact test). (C) ROD^{GFP} localization in wild-type,
775 *Spindly*^{RNAi}, and *nudE*^{RNAi} oocytes with ROD^{GFP} in green, DNA in blue, CENP-C in white,
776 and tubulin in red. Single channel images (bottom) show ROD^{GFP}. Arrow points to
777 abnormal streaming in the *Spindly*^{RNAi} oocyte. See also Figure S 6A. (D) Percent of
778 oocytes with ROD^{GFP} streaming in indicated genotypes (from left to right, n = 25, 41,
779 and 10 oocytes); ns=no significance (Fisher's exact test). (E) Percent of oocytes that
780 abnormal streaming, defined as ROD^{GFP} in the central spindle, in wild-type or
781 *Spindly*^{RNAi} oocytes (n=24 and 43 oocytes); ***P=0.0002 (Fisher's exact test). Abnormal
782 streaming is defined as having ROD^{GFP} in the central region between the centromeres.
783 (F) Quantification of ROD^{GFP} intensity at kinetochores, normalized to background GFP
784 signal in indicated oocytes (from left to right, n = 142, 256, and 72 kinetochores. Error
785 bars show mean ± s.d.; ns=no significance (unpaired two-tailed t test). All images are
786 maximum intensity projections of z stacks. Scale bars represent 5 µm.
787

788

789 Figure S 1. **Validation of *rod* and *mps1* reagents.**

790 (A) Wild-type oocyte with ROD^{GFP} in green, $ZW10^{HA}$ in red, DNA in blue, and tubulin in
791 white. Single channel images show ROD^{GFP} (middle) and $ZW10^{HA}$ (right). (B) ROD^{GFP}
792 localization in wild-type and rod^{RNAi} oocytes with ROD^{GFP} in green, DNA in blue, CENP-
793 C in white, and tubulin in red. Single channel images (right) show ROD^{GFP}. (C)
794 Quantification of ROD^{GFP} intensity at kinetochores, normalized to background GFP
795 signal in wild-type and rod^{RNAi} oocytes (n = 142 and 126 kinetochores). Error bars show
796 mean ± s.d.; ****P<0.0001 (unpaired two-tailed t test). (D) $MPS1^{GFP}$ localization in wild-
797 type and $Mps1^{RNAi}$ oocytes with $MPS1^{GFP}$ in green, DNA in blue, CENP-C in white, and
798 tubulin in red. Single channel images (right) show $MPS1^{GFP}$. (E) Quantification of
799 $MPS1^{GFP}$ intensity at kinetochores, normalized to background GFP signal in wild-type
800 and $Mps1^{RNAi}$ oocytes (n = 75 and 71 kinetochores). Error bars show mean ± s.d.;
801 ****P<0.0001 (unpaired two-tailed t test). All images are maximum intensity projections
802 of z stacks. Scale bars represent 5 µm.
803
804 Figure S 2. **MAD1 and INCENP localization depends on SPC105R.**

805 Control ($Spc105R^{B}$) or mutant oocytes were incubated for one hour in 250 µM
806 colchicine. (A) $MAD1^{GFP}$ (green) localization in indicated genotypes, with DNA in blue,
807 CENP-C in white, and tubulin in red. Single channel images (bottom) show $MAD1^{GFP}$.
808 (B) Quantification of $MAD1^{GFP}$ intensity at kinetochores, normalized to background GFP
809 signal (from left to right, n = 91, 256, 224, 174, 212, 208, and 236 kinetochores). Error
810 bars show mean ± s.d.; ****P<0.0001, ***P=0.0006 (unpaired two-tailed t test). (C)
811 INCENP localization (green) in indicated genotypes with DNA in blue, CENP-C in white,
812 and tubulin in red. Single channel images (bottom) show INCENP. (D) Quantification of
813 INCENP presence at kinetochores (from left to right, n = 16, 29, 11, 31, 20, 18, 21, and
814 11 oocytes). Error bars show mean ± s.d.; ****P<0.0001, *P=0.02 (Fisher's exact test).
815 All images are maximum intensity projections of z stacks. Scale bars represent 5 µm. All
816 *Spc105R* mutants are in an $Spc105R^{RNAi}$ background targeting the endogenous
817 *Spc105R*.
818
819 Figure S 3. **Structure of SPC105R and mutant variants.**

820 A schematic of the *Spc105R* mutants used in this study. The coordinates on the
821 schematic represent the first amino acid of each domain. The N-terminal includes SLRK
822 and RISF. Following this is a domain with three MELT-like motifs, a region that contains
823 two KI-like repeats, a central domain containing repeats with the consensus ExxEED,
824 and the C-terminal region containing coiled-coil motifs.
825
826 Figure S 4. **MPS1 localization depends on SPC105R and NDC80.**

827 (A) $MPS1^{GFP}$ localization in wild-type, $Spc105R^{RNAi}$, and $Ndc80^{RNAi}$ oocytes, with
828 $MPS1^{GFP}$ in green, DNA in blue, CENP-C in white, and tubulin in red. Single channel
829 images (bottom) show $MPS1^{GFP}$. (B) Quantification of $MPS1^{GFP}$ intensity at
830 kinetochores, normalized to background GFP signal in indicated oocytes (from left to

right, n = 389, 195, 139, 160, 165, 198, 128, and 143 kinetochores). Error bars show mean ± s.d.; ****P<0.0001 (unpaired two-tailed t test). (C) Quantification of MPS1^{GFP} intensity at kinetochores, normalized to background GFP signal in wild-type and *Ndc80*^{RNAi} oocytes (n=114 and 148 kinetochores). Error bars show mean ± s.d.; ****P<0.0001 (unpaired two-tailed t test). (D) MPS1^{GFP} localization in the indicated *Spc105R* mutants with MPS1^{GFP} in green, DNA in blue, CENP-C in white, and tubulin in red. All mutants are in an *Spc105R*^{RNAi} background targeting the endogenous *Spc105R*. Single channel images (bottom) show MPS1^{GFP}. All images are maximum intensity projections of z stacks. Scale bars represent 5 μm.

Figure S 5. **ROD and SPC105R localization in *Zw10-Spc105R*^{C} oocytes.**

(A) SPC105R localization in *Zw10-Spc105R*^{C}, either in the presence or absence of *Spc105R*^{RNAi}. SPC105R (green) was detected using an antibody which recognizes the N-terminal regions of SPC105R and does not detect SPC105R^{C}. DNA is in blue, CENP-C in white, and tubulin in red. All images are maximum intensity projections of z stacks. (B) ROD^{GFP} localization in oocytes expressing *Zw10-Spc105R*^{C}, either in the presence or absence of *Spc105R*^{RNAi}. ROD^{GFP} is in green, DNA in blue, CENP-C in white, and tubulin in red. Scale bars represent 5 μm.

Figure S 6. **Localization of Spindly variants and dependence of Spindly on ROD.**

(A) Examples of normal (left) and abnormal (right) ROD^{GFP} streaming in *Spindly*^{RNAi} oocytes, with ROD^{GFP} in green, DNA in blue, CENP-C in white, and tubulin in red. Single channel images (bottom) show ROD^{GFP}. Arrow points to abnormal streaming, which is defined as having ROD^{GFP} in the central region between the centromeres. (B) Spindly^{GFP} localization in wild-type or mutants of *Spindly*. Spindly^{GFP} is in green, DNA in blue, CENP-C in white, and tubulin in red. (C) Localization of Spindly$^{\Delta SB.GFP}$ in *rod*^{RNAi} oocytes, with Spindly^{GFP} in green, DNA in blue, CENP-C in white, and tubulin in red. Spindly^{GFP} and CENP-C are shown below the merged images. All images are maximum intensity projections of z stacks. Scale bars represent 5 μm. (D) Quantification of Spindly^{GFP} intensity at kinetochores in the indicated oocytes (from left to right, n = 123, 164, 83, and 75 kinetochores). Error bars show mean ± s.d.; ****P<0.0001 (unpaired two-tailed t test).

References

1. McAinsh AD, Kops G. Principles and dynamics of spindle assembly checkpoint signalling. Nat Rev Mol Cell Biol. 2023;24(8):543-59. Epub 20230324. doi: 10.1038/s41580-023-00593-z. PubMed PMID: 36964313.
2. Lara-Gonzalez P, Pines J, Desai A. Spindle assembly checkpoint activation and silencing at kinetochores. Seminars in cell & developmental biology. 2021;117:86-98. Epub 20210629. doi: 10.1016/j.semcdb.2021.06.009. PubMed PMID: 34210579; PubMed Central PMCID: PMCPMC8406419.
3. Krenn V, Musacchio A. The Aurora B Kinase in Chromosome Bi-Orientation and Spindle Checkpoint Signaling. Front Oncol. 2015;5:225. Epub 2015/11/04. doi: 10.3389/fonc.2015.00225. PubMed PMID: 26528436; PubMed Central PMCID: PMCPMC4607871.
4. Barbosa J, Sunkel CE, Conde C. The Role of Mitotic Kinases and the RZZ Complex in Kinetochore-Microtubule Attachments: Doing the Right Link. Front Cell Dev Biol. 2022;10:787294. Epub 20220128. doi: 10.3389/fcell.2022.787294. PubMed PMID: 35155423; PubMed Central PMCID: PMCPMC8832123.
5. Lampson MA, Grishchuk EL. Mechanisms to Avoid and Correct Erroneous Kinetochore-Microtubule Attachments. Biology (Basel). 2017;6(1). Epub 2017/01/10. doi: 10.3390/biology6010001. PubMed PMID: 28067761; PubMed Central PMCID: PMCPMC5371994.
6. Kitajima TS. Mechanisms of kinetochore-microtubule attachment errors in mammalian oocytes. Dev Growth Differ. 2018;60(1):33-43. Epub 2018/01/11. doi: 10.1111/dgd.12410. PubMed PMID: 29318599.
7. Mihajlovic AI, FitzHarris G. Segregating Chromosomes in the Mammalian Oocyte. Curr Biol. 2018;28(16):R895-R907. Epub 2018/08/22. doi: 10.1016/j.cub.2018.06.057. PubMed PMID: 30130515.
8. Webster A, Schuh M. Mechanisms of Aneuploidy in Human Eggs. Trends Cell Biol. 2017;27(1):55-68. Epub 2016/10/25. doi: 10.1016/j.tcb.2016.09.002. PubMed PMID: 27773484.
9. Charalambous C, Webster A, Schuh M. Aneuploidy in mammalian oocytes and the impact of maternal ageing. Nat Rev Mol Cell Biol. 2023;24(1):27-44. Epub 20220906. doi: 10.1038/s41580-022-00517-3. PubMed PMID: 36068367.
10. Touati SA, Wassmann K. How oocytes try to get it right: spindle checkpoint control in meiosis. Chromosoma. 2016;125(2):321-35. Epub 20150811. doi: 10.1007/s00412-015-0536-7. PubMed PMID: 26255654.
11. Wu T, Gu H, Luo Y, Wang L, Sang Q. Meiotic defects in human oocytes: Potential causes and clinical implications. Bioessays. 2022;44(12):e2200135. Epub 20221007. doi: 10.1002/bies.202200135. PubMed PMID: 36207289.
12. Liu D, Shao H, Wang H, Liu XJ. Meiosis I in Xenopus oocytes is not error-prone despite lacking spindle assembly checkpoint. Cell Cycle. 2014;13(10):1602-6. Epub 20140319. doi: 10.4161/cc.28562. PubMed PMID: 24646611; PubMed Central PMCID: PMCPMC4050165.
13. Shao H, Li R, Ma C, Chen E, Liu XJ. Xenopus oocyte meiosis lacks spindle assembly checkpoint control. J Cell Biol. 2013;201(2):191-200. Epub 20130408. doi: 10.1083/jcb.201211041. PubMed PMID: 23569212; PubMed Central PMCID: PMCPMC3628510.
14. Gui L, Homer H. Spindle assembly checkpoint signalling is uncoupled from chromosomal position in mouse oocytes. Development. 2012;139(11):1941-6. PubMed PMID: 22513372.

15. Lane SI, Yun Y, Jones KT. Timing of anaphase-promoting complex activation in mouse oocytes is predicted by microtubule-kinetochore attachment but not by bivalent alignment or tension. Development. 2012;139(11):1947-55. PubMed PMID: 22513370.
16. Kyogoku H, Kitajima TS. The large cytoplasmic volume of oocyte. J Reprod Dev. 2023;69(1):1-9. Epub 20221126. doi: 10.1262/jrd.2022-101. PubMed PMID: 36436912; PubMed Central PMCID: PMCPMC9939283.
17. Radford SJ, Nguyen AL, Schindler K, McKim KS. The chromosomal basis of meiotic acentrosomal spindle assembly and function in oocytes. Chromosoma. 2017;126(3):351-64. Epub 2016/11/12. doi: 10.1007/s00412-016-0618-1. PubMed PMID: 27837282; PubMed Central PMCID: PMCPMC5426991.
18. Blengini CS, Schindler K. Acentriolar spindle assembly in mammalian female meiosis and the consequences of its perturbations on human reproduction†. Biol Reprod. 2022;106(2):253-63. doi: 10.1093/biolre/ioab210. PubMed PMID: 34791041; PubMed Central PMCID: PMCPMC8862719.
19. Wartosch L, Schindler K, Schuh M, Gruhn JR, Hoffmann ER, McCoy RC, et al. Origins and mechanisms leading to aneuploidy in human eggs. Prenat Diagn. 2021;41(5):620-30. Epub 20210322. doi: 10.1002/pd.5927. PubMed PMID: 33860956; PubMed Central PMCID: PMCPMC8237340.
20. Singleton MR. Getting to the heart of an unusual kinetochore. Open Biol. 2016;6(4):160040. doi: 10.1098/rsob.160040. PubMed PMID: 27249344; PubMed Central PMCID: PMCPMC4852463.
21. Radford SJ, Hoang TL, Głuszek AA, Ohkura H, McKim KS. Lateral and End-On Kinetochore Attachments Are Coordinated to Achieve Bi-orientation in Drosophila Oocytes. PLoS Genet. 2015;11(10):e1005605. doi: 10.1371/journal.pgen.1005605. PubMed PMID: 26473960.
22. Joshi JN, Changela N, Mahal L, Jang J, Defosse T, Wang LI, et al. Meiosis-specific functions of kinetochore protein SPC105R required for chromosome segregation in Drosophila oocytes. Mol Biol Cell. 2024:mbcE24020067. Epub 20240612. doi: 10.1091/mbc.E24-02-0067. PubMed PMID: 38865189.
23. Cheerambathur DK, Gassmann R, Cook B, Oegema K, Desai A. Crosstalk between microtubule attachment complexes ensures accurate chromosome segregation. Science. 2013;342(6163):1239-42. Epub 2013/11/16. doi: 10.1126/science.1246232. PubMed PMID: 24231804; PubMed Central PMCID: PMCPMC3885540.
24. Barbosa J, Martins T, Bange T, Tao L, Conde C, Sunkel C. Polo regulates Spindly to prevent premature stabilization of kinetochore-microtubule attachments. EMBO J. 2020;39(2):e100789. Epub 2019/12/19. doi: 10.15252/embj.2018100789. PubMed PMID: 31849090; PubMed Central PMCID: PMCPMC6960449.
25. Basto R, Scaerou F, Mische S, Wojcik E, Lefebvre C, Gomes R, et al. In vivo dynamics of the rough deal checkpoint protein during Drosophila mitosis. Curr Biol. 2004;14(1):56-61. PubMed PMID: 14711415.
26. Williams BC, Gatti M, Goldberg ML. Bipolar spindle attachments affect redistributions of ZW10, a Drosophila centromere/kinetochore component required for accurate chromosome segregation. J Cell Biol. 1996;134(5):1127-40. doi: 10.1083/jcb.134.5.1127. PubMed PMID: 8794856; PubMed Central PMCID: PMCPMC2120981.
27. Scaërou F, Starr DA, Piano F, Papoulas O, Karess RE, Goldberg ML. The ZW10 and Rough Deal checkpoint proteins function together in a large, evolutionarily conserved complex targeted to the kinetochore. J Cell Sci. 2001;114(Pt 17):3103-14. doi: 10.1242/jcs.114.17.3103. PubMed PMID: 11590237.
28. Kops G, Gassmann R. Crowning the Kinetochore: The Fibrous Corona in Chromosome Segregation. Trends Cell Biol. 2020;30(8):653-67. Epub 2020/05/11. doi: 10.1016/j.tcb.2020.04.006. PubMed PMID: 32386879.

964 29. Pereira C, Reis RM, Gama JB, Celestino R, Cheerambathur DK, Carvalho AX, et al.
965 Self-Assembly of the RZZ Complex into Filaments Drives Kinetochore Expansion in the
966 Absence of Microtubule Attachment. Current biology : CB. 2018;28(21):3408-21.e8. Epub
967 2018/11/13. doi: 10.1016/j.cub.2018.08.056. PubMed PMID: 30415699; PubMed Central
968 PMCID: PMCPMC6224608.
969 30. Marston AL, Wassmann K. Multiple Duties for Spindle Assembly Checkpoint Kinases in
970 Meiosis. Front Cell Dev Biol. 2017;5:109. Epub 20171213. doi: 10.3389/fcell.2017.00109.
971 PubMed PMID: 29322045; PubMed Central PMCID: PMCPMC5733479.
972 31. Wang LI, DeFosse T, Jang JK, Battaglia RA, Wagner VF, McKim KS. Borealin directs
973 recruitment of the CPC to oocyte chromosomes and movement to the microtubules. J Cell Biol.
974 2021;220(6). Epub 2021/04/10. doi: 10.1083/jcb.202006018. PubMed PMID: 33836043.
975 32. Radford SJ, Jang JK, McKim KS. The Chromosomal Passenger Complex is required for
976 Meiotic Acentrosomal Spindle Assembly and Chromosome Bi-orientation. Genetics.
977 2012;192:417-29. PubMed PMID: 22865736.
978 33. McKim KS, Jang JK, Theurkauf WE, Hawley RS. Mechanical basis of meiotic
979 metaphase arrest. Nature. 1993;362(6418):364-6. PubMed PMID: 8455723.
980 34. Saurin AT. Kinase and Phosphatase Cross-Talk at the Kinetochore. Front Cell Dev Biol.
981 2018;6:62. Epub 2018/07/05. doi: 10.3389/fcell.2018.00062. PubMed PMID: 29971233;
982 PubMed Central PMCID: PMCPMC6018199.
983 35. Caldas GV, DeLuca JG. KNL1: bringing order to the kinetochore. Chromosoma.
984 2014;123(3):169-81. doi: 10.1007/s00412-013-0446-5. PubMed PMID: 24310619; PubMed
985 Central PMCID: PMCPMC4032621.
986 36. Hayward D, Alfonso-Pérez T, Cundell MJ, Hopkins M, Holder J, Bancroft J, et al. CDK1-
987 CCNB1 creates a spindle checkpoint-permissive state by enabling MPS1 kinetochore
988 localization. J Cell Biol. 2019;218(4):1182-99. Epub 20190123. doi: 10.1083/jcb.201808014.
989 PubMed PMID: 30674582; PubMed Central PMCID: PMCPMC6446832.
990 37. Gilliland WD, Hughes SE, Cotitta JL, Takeo S, Xiang Y, Hawley RS. The multiple roles
991 of mps1 in Drosophila female meiosis. PLoS Genet. 2007;3(7):e113. doi:
992 10.1371/journal.pgen.0030113. PubMed PMID: 17630834; PubMed Central PMCID:
993 PMCPMC1914070.
994 38. Gilliland WD, Wayson SM, Hawley RS. The meiotic defects of mutants in the Drosophila
995 mps1 gene reveal a critical role of Mps1 in the segregation of achiasmate homologs. Curr Biol.
996 2005;15(7):672-7. doi: 10.1016/j.cub.2005.02.062. PubMed PMID: 15823541.
997 39. Bourouh M, Dhaliwal R, Rana K, Sinha S, Guo Z, Swan A. Distinct and Overlapping
998 Requirements for Cyclins A, B and B3 in Drosophila Female Meiosis. G3 (Bethesda, Md. 2016.
999 doi: 10.1534/g3.116.033050. PubMed PMID: 27652889; PubMed Central PMCID:
1000 PMCPMC5100870.
1001 40. Malmanche N, Owen S, Gegick S, Steffensen S, Tomkiel JE, Sunkel CE. Drosophila
1002 BubR1 is essential for meiotic sister-chromatid cohesion and maintenance of synaptonemal
1003 complex. Curr Biol. 2007;17(17):1489-97. PubMed PMID: 17702574.
1004 41. Buffin E, Emre D, Karess RE. Flies without a spindle checkpoint. Nat Cell Biol.
1005 2007;9(5):565-72. doi: 10.1038/ncb1570. PubMed PMID: 17417628.
1006 42. Emre D, Terracol R, Poncet A, Rahmani Z, Karess RE. A mitotic role for Mad1 beyond
1007 the spindle checkpoint. J Cell Sci. 2011;124(Pt 10):1664-71. Epub 20110421. doi:
1008 10.1242/jcs.081216. PubMed PMID: 21511728.
1009 43. Hughes SE, Miller DE, Miller AL, Hawley RS. Female Meiosis: Synapsis,
1010 Recombination, and Segregation in Drosophila melanogaster. Genetics. 2018;208(3):875-908.
1011 Epub 2018/03/01. doi: 10.1534/genetics.117.300081. PubMed PMID: 29487146; PubMed
1012 Central PMCID: PMCPMC5844340.

1013 44. Theurkauf WE, Hawley RS. Meiotic spindle assembly in Drosophila females: behavior of
1014 nonexchange chromosomes and the effects of mutations in the nod kinesin-like protein. J Cell
1015 Biol. 1992;116(5):1167-80. PubMed PMID: 1740471.
1016 45. Costa MFA, Ohkura H. The molecular architecture of the meiotic spindle is remodeled
1017 during metaphase arrest in oocytes. J Cell Biol. 2019;218(9):2854-64. Epub 2019/07/07. doi:
1018 10.1083/jcb.201902110. PubMed PMID: 31278080; PubMed Central PMCID:
1019 PMCPMC6719438.
1020 46. Carpenter AT, Sandler L. On recombination-defective meiotic mutants in Drosophila
1021 melanogaster. Genetics. 1974;76(3):453-75. PubMed PMID: 4208856.
1022 47. Jang JK, Gladstein AC, Das A, Shapiro JG, Sisco ZL, McKim KS. Multiple pools of PP2A
1023 regulate spindle assembly, kinetochore attachments, and cohesion in Drosophila oocytes. J Cell
1024 Sci. 2021;134(14):jcs254037. Epub 2021/06/24. doi: 10.1242/jcs.254037. PubMed PMID:
1025 34160620.
1026 48. Wu J, Larreategui-Aparicio A, Lambers MLA, Bodor DL, Klaasen SJ, Tollenaar E, et al.
1027 Microtubule nucleation from the fibrous corona by LIC1-pericentrin promotes chromosome
1028 congression. Curr Biol. 2023;33(5):912-25 e6. Epub 20230130. doi: 10.1016/j.cub.2023.01.010.
1029 PubMed PMID: 36720222; PubMed Central PMCID: PMCPMC10017265.
1030 49. Menant A, Karess RE. Mutations in the Drosophila rough deal gene affecting RZZ
1031 kinetochore function. Biol Cell. 2020;112(10):300-15. Epub 20200720. doi:
1032 10.1111/boc.201900105. PubMed PMID: 32602944.
1033 50. Wojcik E, Basto R, Serr M, Scaërou F, Karess R, Hays T. Kinetochore dynein: its
1034 dynamics and role in the transport of the Rough deal checkpoint protein. Nature cell biology.
1035 2001;3(11):1001-7. Epub 2001/11/21. doi: 10.1038/ncb1101-1001. PubMed PMID: 11715021.
1036 51. Griffis ER, Stuurman N, Vale RD. Spindly, a novel protein essential for silencing the
1037 spindle assembly checkpoint, recruits dynein to the kinetochore. J Cell Biol. 2007;177(6):1005-
1038 15. doi: 10.1083/jcb.200702062. PubMed PMID: 17576797; PubMed Central PMCID:
1039 PMCPMC2064361.
1040 52. Wainman A, Creque J, Williams B, Williams EV, Bonaccorsi S, Gatti M, et al. Roles of
1041 the Drosophila NudE protein in kinetochore function and centrosome migration. J Cell Sci.
1042 2009;122(Pt 11):1747-58. Epub 2009/05/07. doi: 10.1242/jcs.041798. PubMed PMID:
1043 19417004; PubMed Central PMCID: PMCPMC2684831.
1044 53. Gassmann R, Essex A, Hu JS, Maddox PS, Motegi F, Sugimoto A, et al. A new
1045 mechanism controlling kinetochore-microtubule interactions revealed by comparison of two
1046 dynein-targeting components: SPDL-1 and the Rod/Zwilch/Zw10 complex. Genes Dev.
1047 2008;22(17):2385-99. doi: 10.1101/gad.1687508. PubMed PMID: 18765790; PubMed Central
1048 PMCID: PMCPMC2532926.
1049 54. Clemente GD, Hannaford MR, Beati H, Kapp K, Januschke J, Griffis ER, et al.
1050 Requirement of the Dynein-Adaptor Spindly for Mitotic and Post-Mitotic Functions in Drosophila.
1051 J Dev Biol. 2018;6(2). Epub 2018/04/05. doi: 10.3390/jdb6020009. PubMed PMID: 29615558;
1052 PubMed Central PMCID: PMCPMC6027351.
1053 55. Davis-Roca AC, Muscat CC, Wignall SM. Caenorhabditis elegans oocytes detect meiotic
1054 errors in the absence of canonical end-on kinetochore attachments. J Cell Biol.
1055 2017;216(5):1243-53. Epub 20170329. doi: 10.1083/jcb.201608042. PubMed PMID: 28356326;
1056 PubMed Central PMCID: PMCPMC5412562.
1057 56. Jones KT, Lane SI. Molecular causes of aneuploidy in mammalian eggs. Development.
1058 2013;140(18):3719-30. doi: 10.1242/dev.090589. PubMed PMID: 23981655.
1059 57. Touati SA, Buffin E, Cladiere D, Hached K, Rachez C, van Deursen JM, et al. Mouse
1060 oocytes depend on BubR1 for proper chromosome segregation but not for prophase I arrest.
1061 Nat Commun. 2015;6:6946. Epub 2015/04/22. doi: 10.1038/ncomms7946. PubMed PMID:
1062 25897860; PubMed Central PMCID: PMCPMC4439927.

1063 58. Qiao JY, Zhou Q, Xu K, Yue W, Lei WL, Li YY, et al. Mad2 is dispensable for accurate
1064 chromosome segregation but becomes essential when oocytes are subjected to environmental
1065 stress. Development. 2023;150(14). Epub 20230724. doi: 10.1242/dev.201398. PubMed PMID:
1066 37485540.
1067 59. Batiha O, Swan A. Evidence that the spindle assembly checkpoint does not regulate
1068 APC(Fzy) activity in Drosophila female meiosis. Genome. 2012;55(1):63-7. Epub 20111223.
1069 doi: 10.1139/g11-079. PubMed PMID: 22196012.
1070 60. Jang JK, Messina L, Erdman MB, Arbel T, Hawley RS. Induction of metaphase arrest in
1071 Drosophila oocytes by chiasma-based kinetochore tension. Science. 1995;268(5219):1917-9.
1072 61. !!! INVALID CITATION !!! [22, 46].
1073 62. !!! INVALID CITATION !!! [31, 58].
1074 63. !!! INVALID CITATION !!! [60].
1075 64. Silió V, McAinsh AD, Millar JB. KNL1-Bubs and RZZ Provide Two Separable Pathways
1076 for Checkpoint Activation at Human Kinetochores. Dev Cell. 2015;35(5):600-13. Epub
1077 2015/12/15. doi: 10.1016/j.devcel.2015.11.012. PubMed PMID: 26651294.
1078 65. Pauleau AL, Bergner A, Kajtez J, Erhardt S. The checkpoint protein Zw10 connects
1079 CAL1-dependent CENP-A centromeric loading and mitosis duration in Drosophila cells. PLoS
1080 Genet. 2019;15(9):e1008380. Epub 20190925. doi: 10.1371/journal.pgen.1008380. PubMed
1081 PMID: 31553715; PubMed Central PMCID: PMCPMC6779278.
1082 66. O'Tousa J. Meiotic chromosome behavior influenced by mutation-altered disjunction in
1083 Drosophila melanogaster females. Genetics. 1982;102:503-24.
1084 67. Hached K, Xie SZ, Buffin E, Cladiere D, Rachez C, Sacras M, et al. Mps1 at
1085 kinetochores is essential for female mouse meiosis I. Development. 2011;138(11):2261-71.
1086 PubMed PMID: 21558374.
1087 68. Sarangapani KK, Koch LB, Nelson CR, Asbury CL, Biggins S. Kinetochore-bound Mps1
1088 regulates kinetochore-microtubule attachments via Ndc80 phosphorylation. J Cell Biol.
1089 2021;220(12). Epub 20211014. doi: 10.1083/jcb.202106130. PubMed PMID: 34647959;
1090 PubMed Central PMCID: PMCPMC8641409.
1091 69. Hiruma Y, Sacristan C, Pachis ST, Adamopoulos A, Kuijt T, Ubbink M, et al. CELL
1092 DIVISION CYCLE. Competition between MPS1 and microtubules at kinetochores regulates
1093 spindle checkpoint signaling. Science. 2015;348(6240):1264-7. Epub 20150611. doi:
1094 10.1126/science.aaa4055. PubMed PMID: 26068855.
1095 70. Ji Z, Gao H, Yu H. CELL DIVISION CYCLE. Kinetochore attachment sensed by
1096 competitive Mps1 and microtubule binding to Ndc80C. Science. 2015;348(6240):1260-4. doi:
1097 10.1126/science.aaa4029. PubMed PMID: 26068854.
1098 71. Kemmler S, Stach M, Knapp M, Ortiz J, Pfannstiel J, Ruppert T, et al. Mimicking Ndc80
1099 phosphorylation triggers spindle assembly checkpoint signalling. EMBO J. 2009;28(8):1099-
1100 110. Epub 20090319. doi: 10.1038/emboj.2009.62. PubMed PMID: 19300438; PubMed Central
1101 PMCID: PMCPMC2683709.
1102 72. Hayward D, Roberts E, Gruneberg U. MPS1 localizes to end-on microtubule-attached
1103 kinetochores to promote microtubule release. Curr Biol. 2022;32(23):5200-8 e8. Epub
1104 20221116. doi: 10.1016/j.cub.2022.10.047. PubMed PMID: 36395767.
1105 73. Buffin E, Lefebvre C, Huang J, Gagou ME, Karess RE. Recruitment of Mad2 to the
1106 kinetochore requires the Rod/Zw10 complex. Curr Biol. 2005;15(9):856-61. PubMed PMID:
1107 15886105.
1108 74. Kops GJ, Kim Y, Weaver BA, Mao Y, McLeod I, Yates JR, 3rd, et al. ZW10 links mitotic
1109 checkpoint signaling to the structural kinetochore. J Cell Biol. 2005;169(1):49-60. doi:
1110 10.1083/jcb.200411118. PubMed PMID: 15824131; PubMed Central PMCID:
1111 PMCPMC1351127.

1112 75. Tromer E, Snel B, Kops GJ. Widespread Recurrent Patterns of Rapid Repeat Evolution
1113 in the Kinetochore Scaffold KNL1. Genome Biol Evol. 2015;7(8):2383-93. Epub 2015/08/09. doi:
1114 10.1093/gbe/evv140. PubMed PMID: 26254484; PubMed Central PMCID: PMCPMC4558858.
1115 76. Caldas GV, Lynch TR, Anderson R, Afreen S, Varma D, DeLuca JG. The RZZ complex
1116 requires the N-terminus of KNL1 to mediate optimal Mad1 kinetochore localization in human
1117 cells. Open Biol. 2015;5(11). doi: 10.1098/rsob.150160. PubMed PMID: 26581576; PubMed
1118 Central PMCID: PMCPMC4680571.
1119 77. Zhang G, Lischetti T, Hayward DG, Nilsson J. Distinct domains in Bub1 localize RZZ and
1120 BubR1 to kinetochores to regulate the checkpoint. Nat Commun. 2015;6:7162. Epub 20150602.
1121 doi: 10.1038/ncomms8162. PubMed PMID: 26031201; PubMed Central PMCID:
1122 PMCPMC4458899.
1123 78. McGory JM, Verma V, Barcelos DM, Maresca TJ. Multimerization of a disordered
1124 kinetochore protein promotes accurate chromosome segregation by localizing a core dynein
1125 module. J Cell Biol. 2024;223(3). Epub 20240105. doi: 10.1083/jcb.202211122. PubMed PMID:
1126 38180477; PubMed Central PMCID: PMCPMC10770731.
1127 79. Davydenko O, Schultz RM, Lampson MA. Increased CDK1 activity determines the timing
1128 of kinetochore-microtubule attachments in meiosis I. J Cell Biol. 2013;202(2):221-9. doi:
1129 10.1083/jcb.201303019. PubMed PMID: 23857768; PubMed Central PMCID:
1130 PMCPMC3718970.
1131 80. Kabeche L, Compton DA. Cyclin A regulates kinetochore microtubules to promote
1132 faithful chromosome segregation. Nature. 2013;502(7469):110-3. doi: 10.1038/nature12507.
1133 PubMed PMID: 24013174; PubMed Central PMCID: PMCPMC3791168.
1134 81. Amin MA, McKenney RJ, Varma D. Antagonism between the dynein and Ndc80
1135 complexes at kinetochores controls the stability of kinetochore-microtubule attachments during
1136 mitosis. J Biol Chem. 2018;293(16):5755-65. Epub 2018/02/25. doi: 10.1074/jbc.RA117.001699.
1137 PubMed PMID: 29475948; PubMed Central PMCID: PMCPMC5912454.
1138 82. Sacristan C, Ahmad MUD, Keller J, Fermie J, Groenewold V, Tromer E, et al. Dynamic
1139 kinetochore size regulation promotes microtubule capture and chromosome biorientation in
1140 mitosis. Nat Cell Biol. 2018;20(7):800-10. Epub 2018/06/20. doi: 10.1038/s41556-018-0130-3.
1141 PubMed PMID: 29915359; PubMed Central PMCID: PMCPMC6485389.
1142 83. Wang LI, Das A, McKim KS. Sister centromere fusion during meiosis I depends on
1143 maintaining cohesins and destabilizing microtubule attachments. PLoS Genet.
1144 2019;15(5):e1008072. Epub 2019/06/01. doi: 10.1371/journal.pgen.1008072. PubMed PMID:
1145 31150390; PubMed Central PMCID: PMCPMC6581285.
1146 84. Barbosa J, Conde C, Sunkel C. RZZ-SPINDLY-DYNEIN: you got to keep 'em separated.
1147 Cell Cycle. 2020;19(14):1716-26. Epub 20200616. doi: 10.1080/15384101.2020.1780382.
1148 PubMed PMID: 32544383; PubMed Central PMCID: PMCPMC7469663.
1149 85. Barisic M, Sohm B, Mikolcevic P, Wandke C, Rauch V, Ringer T, et al. Spindly/CCDC99
1150 is required for efficient chromosome congression and mitotic checkpoint regulation. Mol Biol
1151 Cell. 2010;21(12):1968-81. Epub 2010/04/30. doi: 10.1091/mbc.E09-04-0356. PubMed PMID:
1152 20427577; PubMed Central PMCID: PMCPMC2883941.
1153 86. Gassmann R, Holland AJ, Varma D, Wan X, Civril F, Cleveland DW, et al. Removal of
1154 Spindly from microtubule-attached kinetochores controls spindle checkpoint silencing in human
1155 cells. Genes & development. 2010;24(9):957-71. Epub 2010/05/05. doi: 10.1101/gad.1886810.
1156 PubMed PMID: 20439434; PubMed Central PMCID: PMCPMC2861194.
1157 87. Wu J, Raas MWD, Alcaraz PS, Vos HR, Tromer EC, Snel B, et al. A farnesyl-dependent
1158 structural role for CENP-E in expansion of the fibrous corona. J Cell Biol. 2024;223(1). Epub
1159 20231107. doi: 10.1083/jcb.202303007. PubMed PMID: 37934467; PubMed Central PMCID:
1160 PMCPMC10630089.
1161 88. McGory JM, Verma V, Barcelos DM, Maresca TJ. Multimerization of a disordered
1162 kinetochore protein promotes accurate chromosome segregation by localizing a core dynein

1163 module. J Cell Biol. 2024;223(3):e202211122. Epub 20240105. doi: 10.1083/jcb.202211122.
1164 PubMed PMID: 38180477; PubMed Central PMCID: PMCPMC10770731.
1165 89. Cmentowski V, Ciossani G, d'Amico E, Wohlgemuth S, Owa M, Dynlacht B, et al. RZZ-
1166 Spindly and CENP-E form an integrated platform to recruit dynein to the kinetochore corona.
1167 Embo j. 2023;42(24):e114838. Epub 20231120. doi: 10.15252/embj.2023114838. PubMed
1168 PMID: 37984321; PubMed Central PMCID: PMCPMC10711656.
1169 90. Althoff F, Karess RE, Lehner CF. Spindle checkpoint-independent inhibition of mitotic
1170 chromosome segregation by Drosophila Mps1. Mol Biol Cell. 2012;23(12):2275-91. Epub
1171 20120502. doi: 10.1091/mbc.E12-02-0117. PubMed PMID: 22553353; PubMed Central PMCID:
1172 PMCPMC3374747.
1173 91. Fischer MG, Heeger S, Hacker U, Lehner CF. The mitotic arrest in response to hypoxia
1174 and of polar bodies during early embryogenesis requires Drosophila Mps1. Curr Biol.
1175 2004;14(22):2019-24. doi: 10.1016/j.cub.2004.11.008. PubMed PMID: 15556864.
1176 92. Zeng Y, Li H, Schweppe NM, Hawley RS, Gilliland WD. Statistical analysis of
1177 nondisjunction assays in Drosophila. Genetics. 2010;186(2):505-13. doi:
1178 10.1534/genetics.110.118778. PubMed PMID: 20660647; PubMed Central PMCID:
1179 PMCPMC2954469.
1180 93. Défachelles L, Hainline SG, Menant A, Lee LA, Karess RE. A maternal effect rough deal
1181 mutation suggests that multiple pathways regulate Drosophila RZZ kinetochore recruitment. J
1182 Cell Sci. 2015;128(6):1204-16. Epub 20150122. doi: 10.1242/jcs.165712. PubMed PMID:
1183 25616898; PubMed Central PMCID: PMCPMC4359924.
1184 94. Radford SJ, McKim KS. Techniques for Imaging Prometaphase and Metaphase of
1185 Meiosis I in Fixed Drosophila Oocytes. Journal of visualized experiments : JoVE.
1186 2016;116(116):e54666. doi: 10.3791/54666. PubMed PMID: 27842371.
1187 95. Chu DT, Klymkowsky MW. The appearance of acetylated alpha-tubulin during early
1188 development and cellular differentiation in Xenopus. Dev Biol. 1989;136(1):104-17. doi:
1189 10.1016/0012-1606(89)90134-6. PubMed PMID: 2680681.
1190 96. Wu C, Singaram V, McKim KS. mei-38 is required for chromosome segregation during
1191 meiosis in Drosophila females. Genetics. 2008;180(1):61-72. PubMed PMID: 18757915.
1192 97. Fellmeth JE, Jang JK, Persaud M, Sturm H, Changela N, Parikh A, et al. A dynamic
1193 population of prophase CENP-C is required for meiotic chromosome segregation. PLoS Genet.
1194 2023;19(11):e1011066. Epub 20231129. doi: 10.1371/journal.pgen.1011066. PubMed PMID:
1195 38019881.
1196 98. Schittenhelm RB, Chaleckis R, Lehner CF. Intrakinetochore localization and essential
1197 functional domains of Drosophila Spc105. EMBO J. 2009;28(16):2374-86. doi:
1198 10.1038/emboj.2009.188. PubMed PMID: 19590494; PubMed Central PMCID:
1199 PMCPMC2735171.
1200 99. Sugimura I, Lilly MA. Bruno inhibits the expression of mitotic cyclins during the prophase
1201 I meiotic arrest of Drosophila oocytes. Dev Cell. 2006;10(1):127-35. PubMed PMID: 16399084.
1202 100. Schittenhelm RB, Heeger S, Althoff F, Walter A, Heidmann S, Mechtler K, et al. Spatial
1203 organization of a ubiquitous eukaryotic kinetochore protein network in Drosophila
1204 chromosomes. Chromosoma. 2007;116(4):385-402. PubMed PMID: 17333235.
1205 101. Ni JQ, Zhou R, Czech B, Liu LP, Holderbaum L, Yang-Zhou D, et al. A genome-scale
1206 shRNA resource for transgenic RNAi in Drosophila. Nature methods. 2011;8(5):405-7. PubMed
1207 PMID: 21460824.
1208 102. Liu H, Jang JK, Graham J, Nycz K, McKim KS. Two genes required for meiotic
1209 recombination in Drosophila are expressed from a dicistronic message. Genetics.
1210 2000;154(4):1735-46.
1211

1212 Figure 1

1213

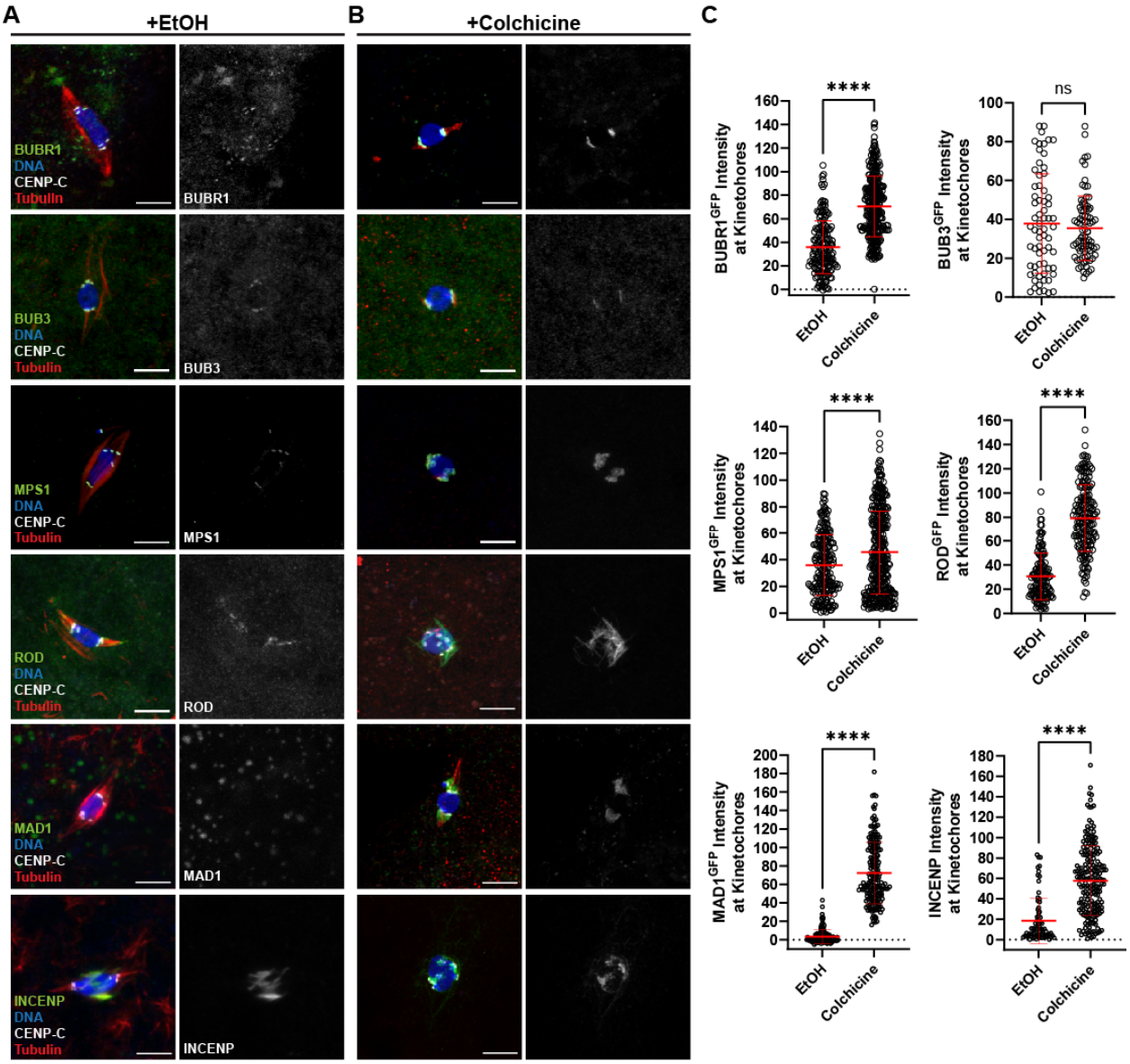

1214

1215

Figure 2

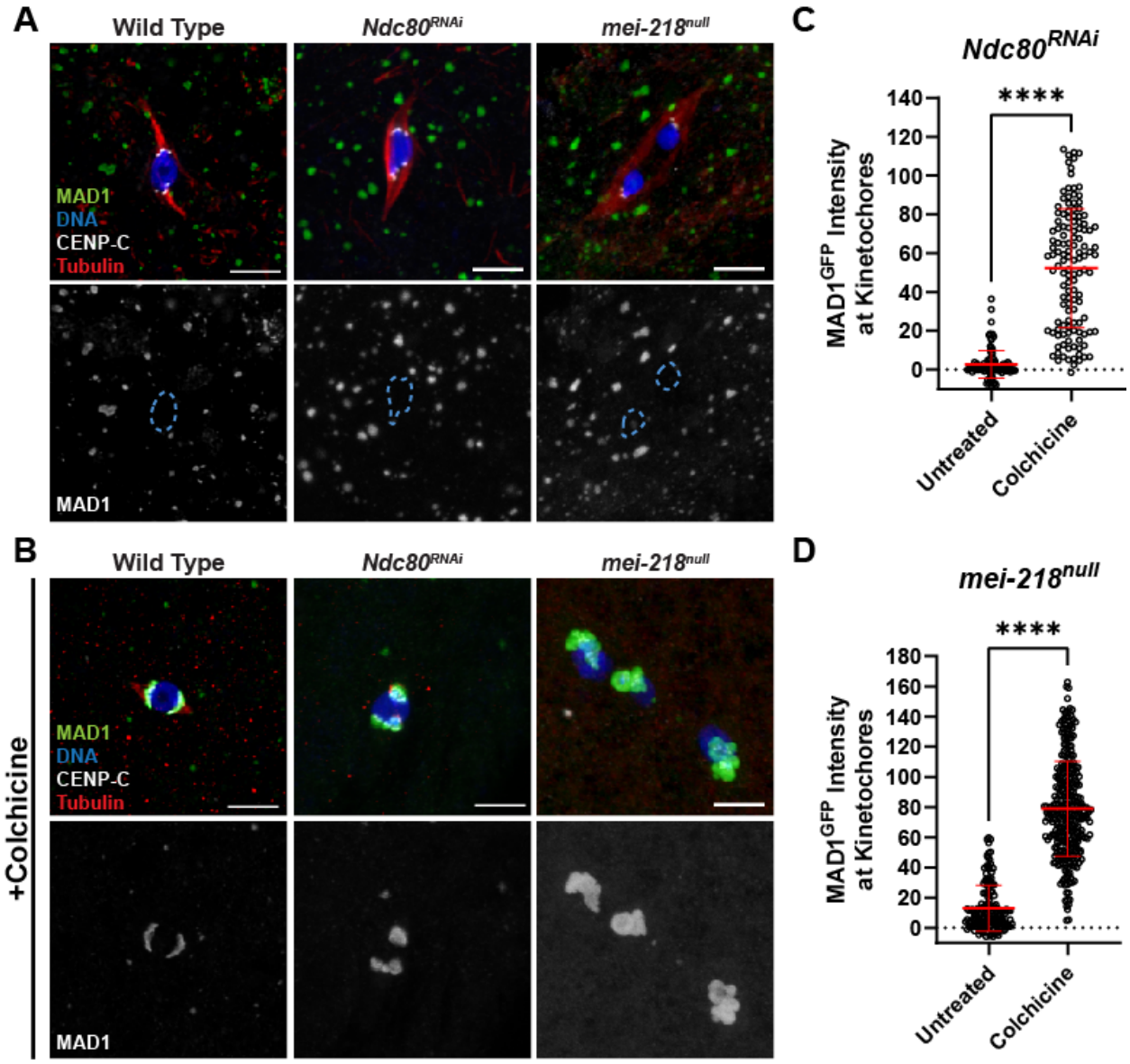
A
Wild Type
Ndc80RNAi
mei-218null
MAD1
DNA
CENP-C
Tubulin
MAD1
B
Wild Type
Ndc80RNAi
mei-218null
+Colchicine
MAD1
DNA
CENP-C
Tubulin
MAD1
C
Ndc80RNAi
****
MAD1GFP Intensity at Kinetochores
140
120
100
80
60
40
20
0
Untreated
Colchicine
D
mei-218null
****
MAD1GFP Intensity at Kinetochores
180
160
140
120
100
80
60
40
20
0
Untreated
Colchicine

Figure 3

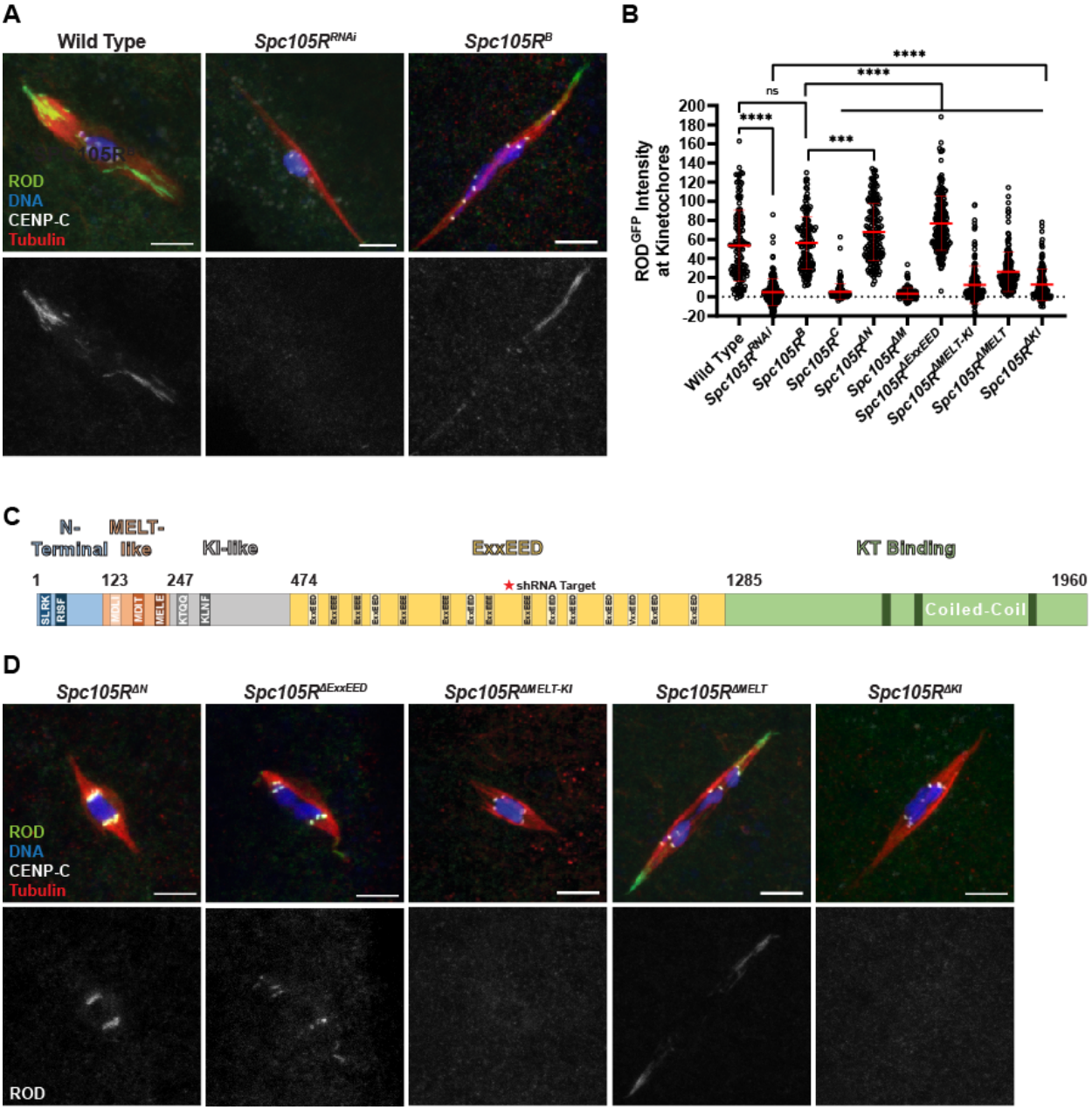
A
Wild Type
Spc105R^RNAi
Spc105R^B
ROD
DNA
CENP-C
Tubulin
B
ROD^GFP Intensity at Kinetochores
Wild Type
Spc105R^RNAi
Spc105R^B
Spc105R^C
Spc105R^ΔN
Spc105R^ΔM
Spc105R^ΔExxEED
Spc105R^ΔMELT-KI
Spc105R^ΔMELT
Spc105R^ΔKI
C
N-Terminal
MELT-like
KI-like
ExxEED
KT Binding
1
123
247
474
1285
1960
shRNA Target
Coiled-Coil
D
Spc105R^ΔN
Spc105R^ΔExxEED
Spc105R^ΔMELT-KI
Spc105R^ΔMELT
Spc105R^ΔKI
ROD
DNA
CENP-C
Tubulin
ROD

1222 Figure 4

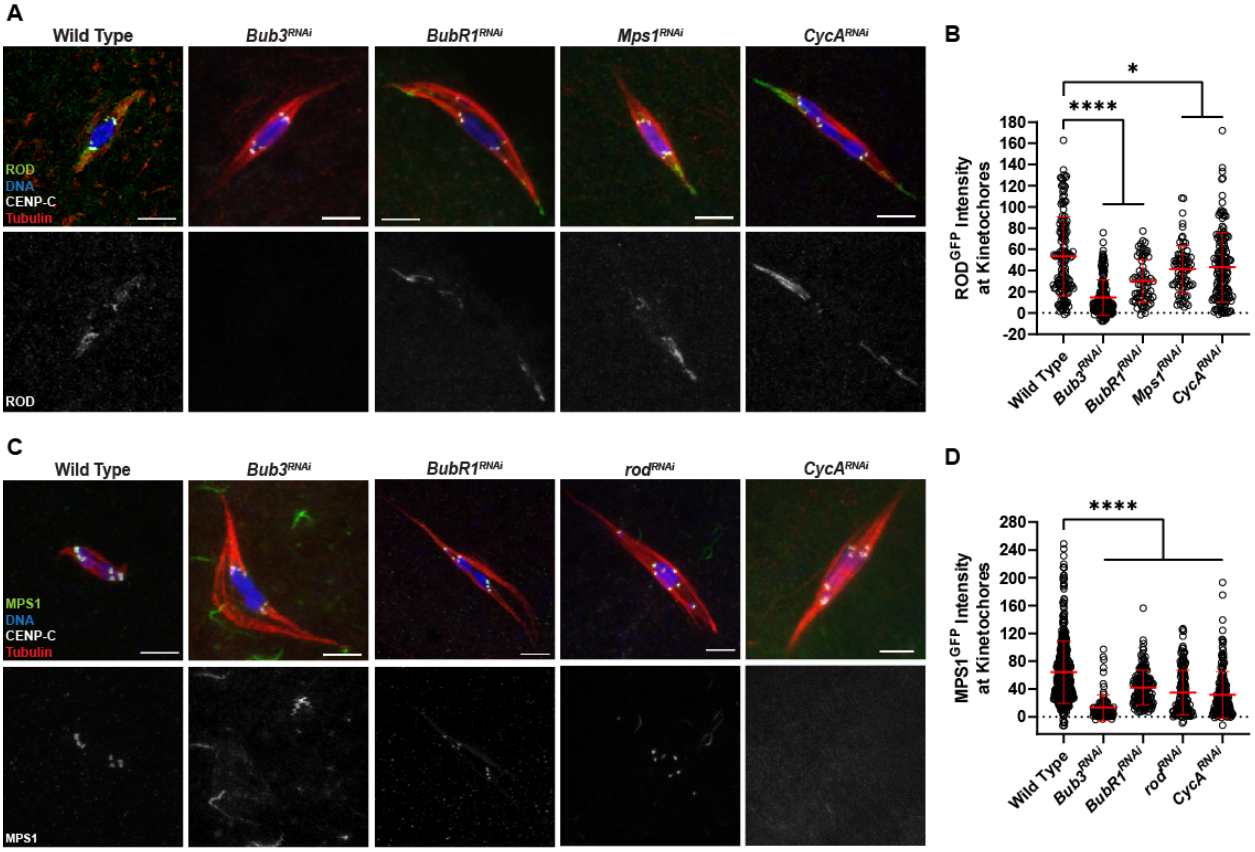

1223

1224

1225 Figure 5

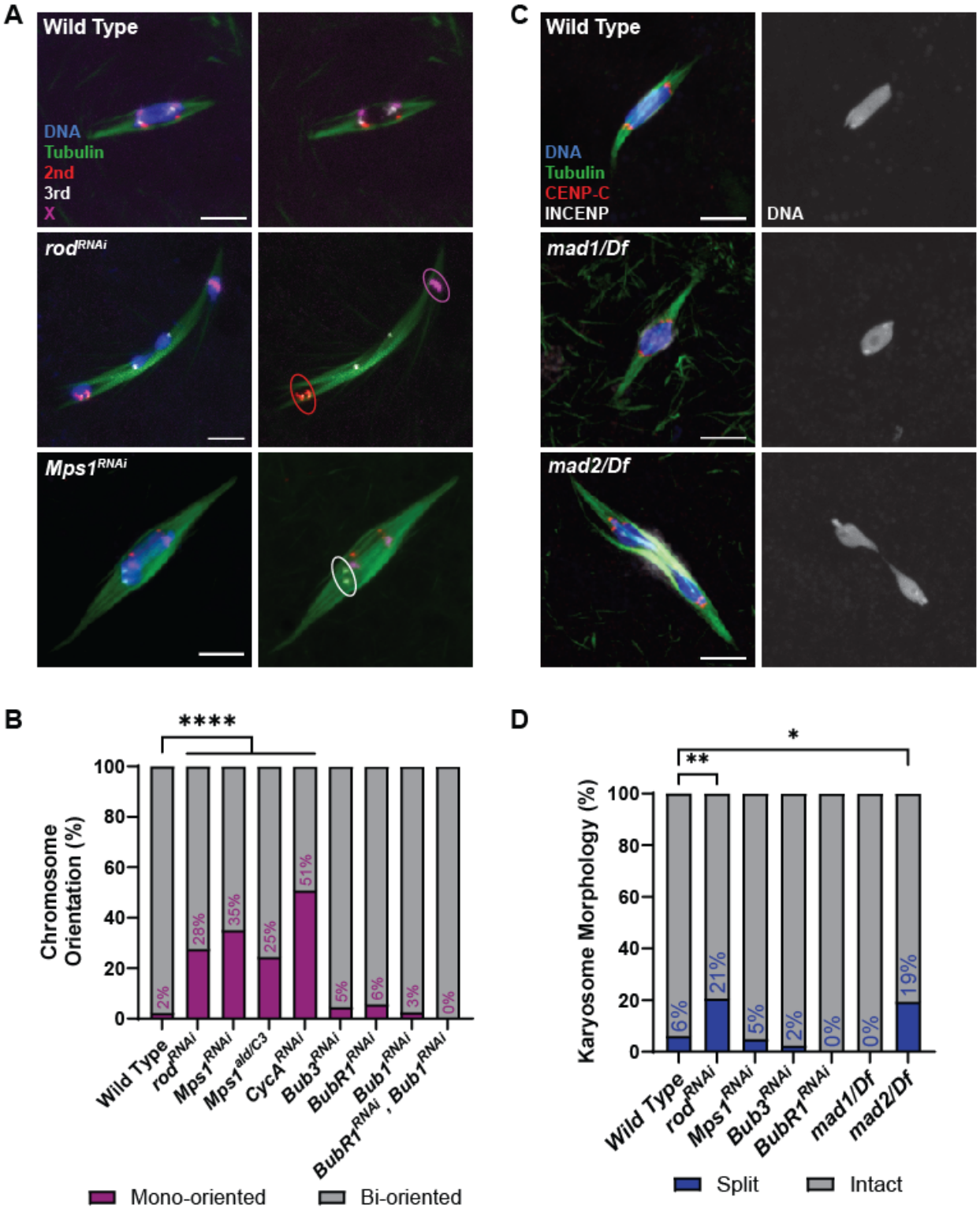

1226

1227

Figure 6

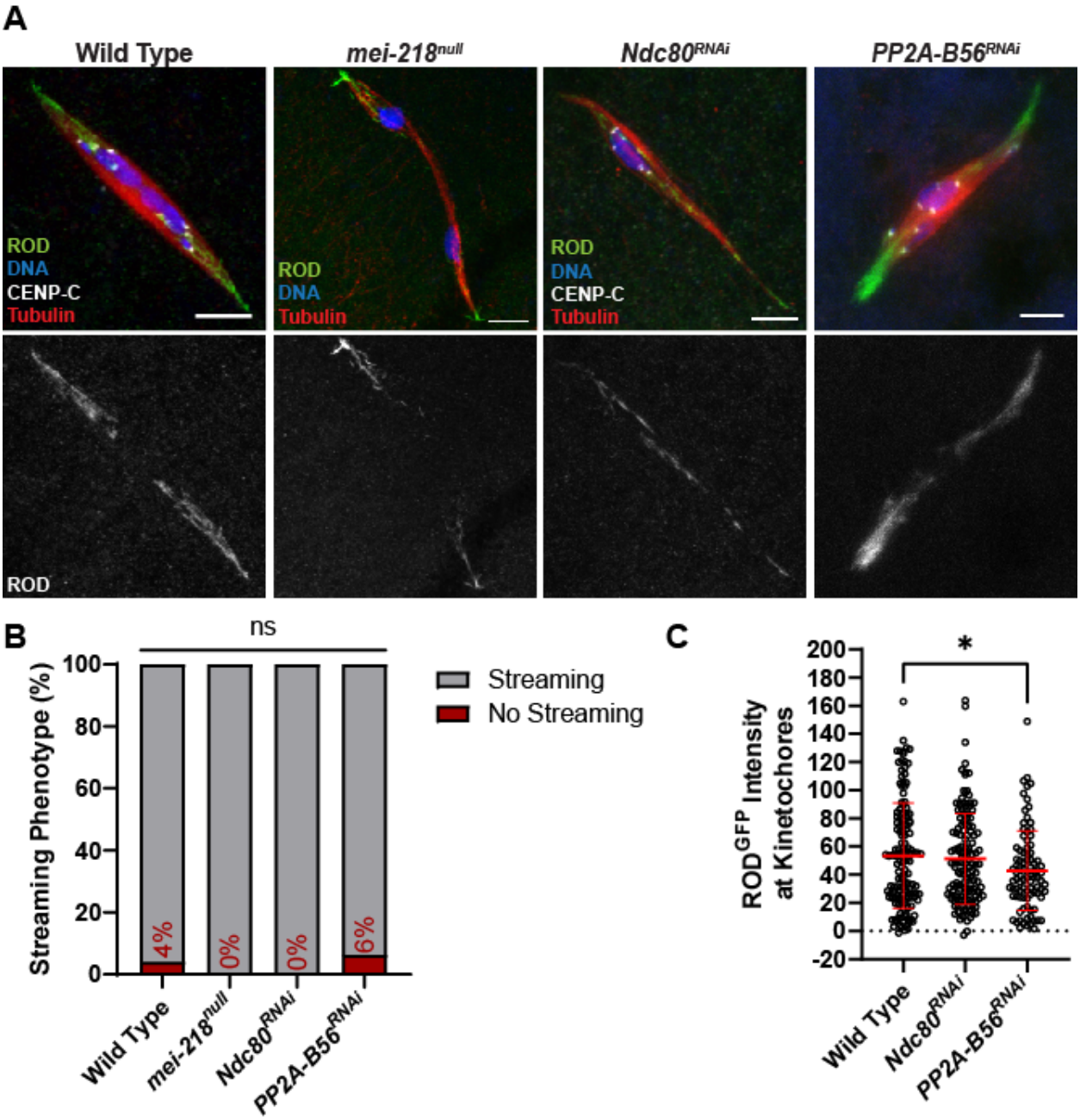
A
Wild Type
mei-218null
Ndc80RNAi
PP2A-B56RNAi
ROD
DNA
CENP-C
Tubulin
ROD
B
ns
Streaming Phenotype (%)
100
80
60
40
20
0
4%
0%
0%
6%
Streaming
No Streaming
Wild Type
mei-218null
Ndc80RNAi
PP2A-B56RNAi
C
*
RODGFP Intensity at Kinetochores
200
180
160
140
120
100
80
60
40
20
0
-20
Wild Type
Ndc80RNAi
PP2A-B56RNAi

1231 Figure 7

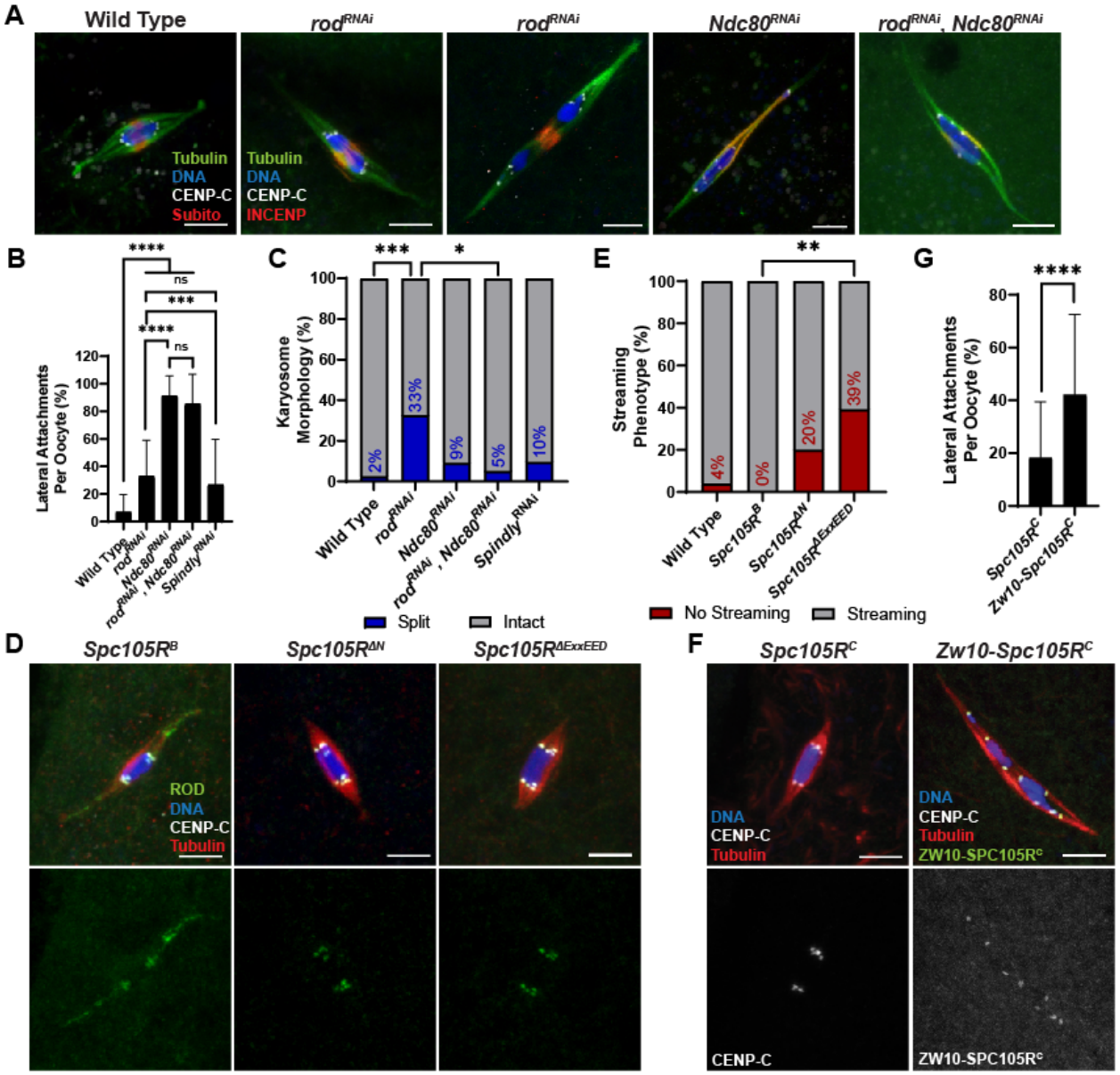

1232

1233

1234

1235

1236 Figure 8

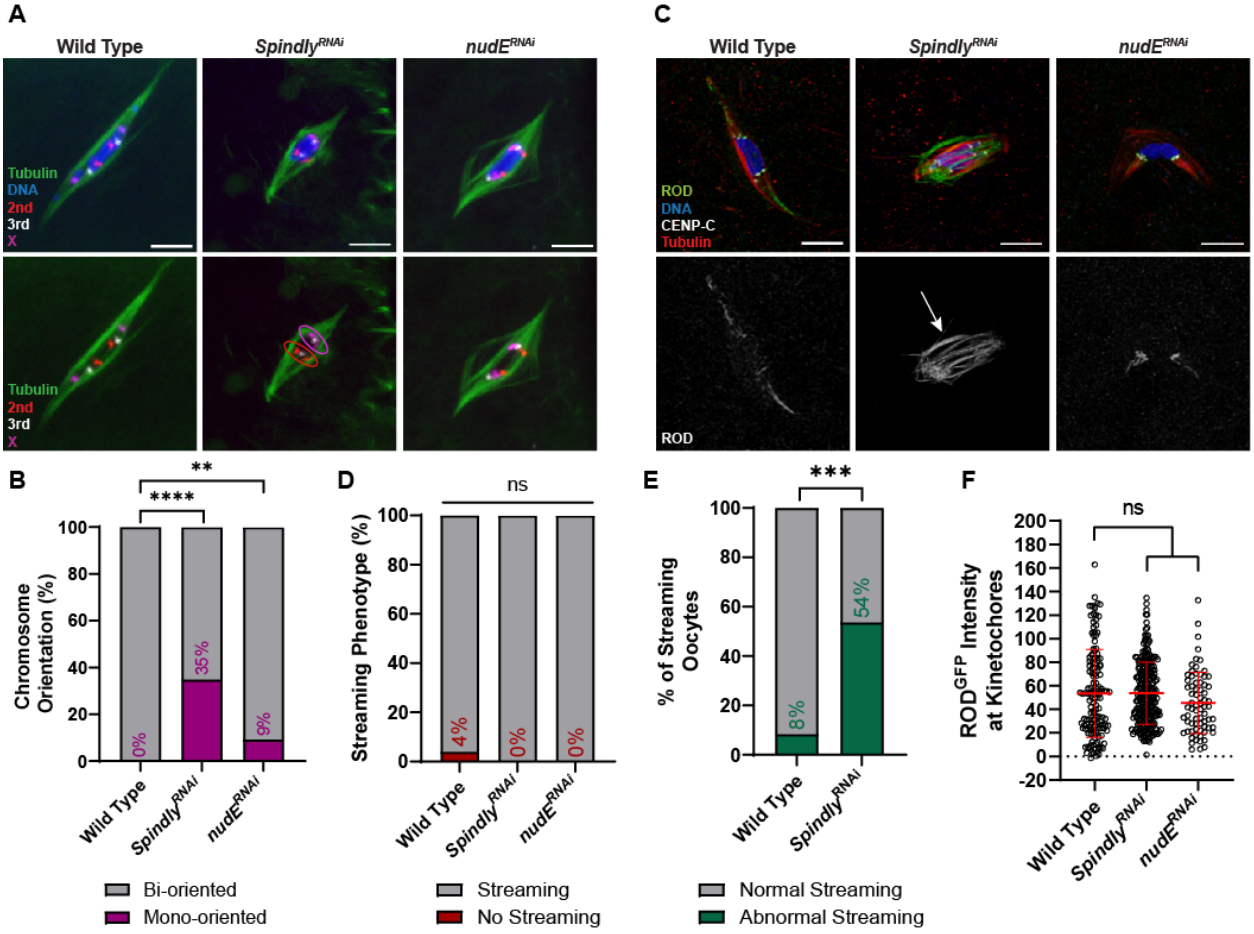

1237

1238